Published in final edited form as:
Sci Transl Med. 2024 February 07; 16(733): eadh8162. doi:10.1126/scitranslmed.adh8162.

Exonic knock-out and knock-in gene editing in hematopoietic stem and progenitor cells rescues RAG1 immunodeficiency

Maria Carmina Castiello[1,2], **Chiara Brandas**[1,3,†], **Samuele Ferrari**[1,†], **Simona Porcellini**[1], **Nicolò Sacchetti**[1,4], **Daniele Canarutto**[1,4,5], **Elena Draghici**[1], **Ivan Merelli**[1,6], **Matteo Barcella**[1,6], **Gabriele Pelosi**[1,4], **Valentina Vavassori**[1], **Angelica Varesi**[1], **Aurelien Jacob**[1], **Serena Scala**[1], **Luca Basso Ricci**[1], **Marianna Paulis**[2,7], **Dario Strina**[2,7], **Martina Di Verniere**[1,2], **Lucia Sergi Sergi**[1], **Marta Serafini**[3,8], **Steven M. Holland**[9], **Jenna R.E. Bergerson**[9], **Suk See De Ravin**[9], **Harry L. Malech**[9], **Francesca Pala**[9], **Marita Bosticardo**[9], **Chiara Brombin**[10], **Federica Cugnata**[10], **Enrica Calzoni**[1], **Gay M. Crooks**[11], **Luigi D. Notarangelo**[9], **Pietro Genovese**[1,12], **Luigi Naldini**[1,4,†], **Anna Villa**[1,2,†,*]

[1.]San Raffaele-Telethon Institute for Gene Therapy (SR-Tiget), IRCSS San Raffaele Scientific Institute, Milan, 20132, Italy.

[2.]Milan Unit, Istituto di Ricerca Genetica e Biomedica (IRGB), Consiglio Nazionale delle Ricerche (CNR), Rozzano (MI), 20089, Italy.

[3.]Translational and Molecular Medicine (DIMET), University of Milano-Bicocca, Monza, 20900, Italy.

[4.]Vita-Salute San Raffaele University, Milan, 20132, Italy.

[5.]Pediatric Immunohematology Unit and BMT Program, IRCCS San Raffaele Scientific Institute, Milan, 20132, Italy.

[*]Corresponding author. villa.anna@hsr.it.
[†]These authors contributed equally to this work

Author contributions: MCC designed the study, performed research, interpreted data, and wrote the manuscript; C. Brandas performed experiments, interpreted data and revised the manuscript; SF designed the study of the exonic gene editing strategy, interpreted data and revised the manuscript; SP performed experiments and interpreted data; NS performed experiments on the intronic gene editing strategy; DC formulated the rationale and designed some experiments on the exonic gene editing strategy; ED provided technical support with in vivo experiments; IM and M. Barcella performed bioinformatic analyses; GP, VV, A. Varesi and AJ provided technical support; SS and LBR performed the multiparametric whole blood dissection assay on HPSCs; MP, DS and MdV provide technical support with in vitro and in vivo experiments; LSS produced the lentiviral vector LV.PGK-iGFP; C. Brombin and FC performed some statistical analyses; MS revised the manuscript; SMH, JREB, SSDR and HLM provided RAG1-patient HSPCs; FP, M. Bosticardo and EC provided technical support with ATO platform; GMC provided MS5 cells for ATO platform; LDN provided scientific discussion and revised the manuscript; PG provided scientific support on the intronic gene editing strategy and revised the manuscript; LN and A. Villa supervised research, coordinated the work and revised the manuscript.

Competing interests: MCC, A. Villa, LN, SF, SP, NS, PG, DC and AJ are inventors of patents ("Polynucleotides useful for correcting mutations in the RAG1 gene", International Publication No. WO2023062030A1, Inventors: A. Villa, LN, SF, MCC, SP, DC. "Replacement of RAG1 for use in therapy", International Publication No. WO2022079054A1, Inventors: A. Villa, PG, LN, NS, MCC, SF. "Enhancing efficiency and tolerability of gene editing in primary cells", International Publication No. WO2020002380A1, Inventors: PG, LN, AJ, SF.) pertaining to the results presented in the paper owned and managed by the San Raffaele Scientific Institute and Telethon Foundation. LN is a founder, equity owner consultant of GeneSpire, a biotechnology startup developing LV-based liver gene transfer and hematopoietic cell gene editing. The other authors declare that they have no competing interests.

LIST OF SUPPLEMENTARY MATERIALS
Materials and Methods
Fig. S1 to S9
Tables S1 to S12
Data files S1 and S2
References (35, 96–99)

[6]National Research Council (CNR), Institute for Biomedical Technologies, Segrate (MI) 20054, Italy.

[7]Humanitas Clinical and Research Center IRCCS, Rozzano (MI), 20089, Italy.

[8]Tettamanti Center, Fondazione IRCCS San Gerardo dei Tintori, Monza (MI), 20900, Italy.

[9]Laboratory of Clinical Immunology and Microbiology, NIAID, NIH, Bethesda, MD, 20892, USA.

[10]University Center for Statistics in the Biomedical Sciences, Vita-Salute San Raffaele University, Milan, 20132, Italy.

[11]Department of Pathology and Laboratory Medicine, David Geffen School of Medicine, Univ. of California, Los Angeles (UCLA), Los Angeles, CA, 90095, USA.

[12]Gene Therapy Program, Dana-Farber/Boston Children's Cancer and Blood Disorders Center, Harvard Medical School, Boston, MA, 02115, USA.

Abstract

Recombination activating genes (*RAGs*) are tightly regulated during lymphoid differentiation, and their mutations cause a spectrum of severe immunological disorders. Haematopoietic stem and progenitor cell (HSPC) transplantation is the treatment of choice but is limited by donor availability and toxicity. To overcome these issues, we developed gene editing strategies targeting a corrective sequence into the human *RAG1* gene by homology-directed repair (HDR) and validated them by tailored 2-dimensional, 3-dimensional and in vivo xenotransplant platforms to assess rescue of expression and function. Whereas integration into intron 1 of *RAG1* achieved suboptimal correction, in-frame insertion into exon 2 drove physiologic human RAG1 expression and activity, allowing disruption of the dominant-negative effects of unrepaired hypomorphic alleles. Enhanced HDR-mediated gene editing enables the correction of human *RAG1* in HSPCs from patients with hypomorphic *RAG1* mutations, allowing the overcome of T- and B-cell differentiation blocks. Gene correction efficiency exceeded the minimal proportion of functional HSPCs required to rescue immunodeficiency in $Rag1^{-/-}$ mice, supporting the clinical translation of HSPC gene editing for the treatment of RAG1 deficiency.

One Sentence Summary:

Gene editing enables rescue of *RAG1* expression and function in human hematopoietic stem and progenitor cells by exploiting homology-directed repair.

INTRODUCTION

Recombination activating genes (RAGs) orchestrate V(D)J recombination, required for lymphocyte development and somatic diversity of the T-cell receptor (TCR) and B-cell receptor (BCR) (1). Loss of function mutations in RAGs result in absence or severe reduction of T and B cells (T-B- severe combined immunodeficiency, SCID), whereas hypomorphic mutations decrease recombination activity, leading to a spectrum of immune dysregulation phenotypes including Omenn Syndrome (OS), leaky SCID with residual T and B cells (2), presence of autoimmune and autoinflammatory manifestations (3–5), and

delayed-onset combined immunodeficiency, often associated with granulomatous and/or autoimmune manifestations (CID-G/AI) (6).

RAG defects accounts for 20% of all SCID cases, and human *RAG1* (*hRAG1*) mutations are more common than *RAG2* mutations (7). Allogeneic hematopoietic stem cell transplantation (HSCT) is the treatment of choice, with optimal results in SCID or OS patients receiving fully HLA-matched donor cells in early life and in the absence of organ damage (8–11). Conversely, unconditioned transplantation from haploidentical donors is associated with a high rate of graft failure (12). Although improved survival has been reported in recent years following haploidentical transplantation with conditioning, graft-versus-host disease and incomplete immune reconstitution remain substantial problems (9, 11). Gene addition to autologous hematopoietic stem and progenitor cells (HSPCs) with retroviral and lentiviral (LV) vectors has been investigated to overcome these limitations (13). Preclinical data showed variable results in terms of immune reconstitution and safety, supporting the need to preserve the endogenous regulation of *hRAG1* expression during cell cycle and lymphoid differentiation (13–18). Gene addition studies in *Rag1*$^{-/-}$ mice based on a lentiviral vector (LV) carrying a codon optimized *hRAG1* (co.hRAG1) cDNA driven by the strong MND promoter derived from a murine γ-retrovirus (14), provided the rationale to start a phase I/II clinical trial to treat T-B- SCID patients up to 2 years old (NCT04797260). Nevertheless, constitutive *hRAG1* expression and genome-wide insertions of a vector bearing powerful transcriptional enhancers raise concerns for the risks to develop immune dysregulation and insertional mutagenesis, respectively (18, 19).

HDR-mediated knock-in of a corrective sequence provides an alternative approach (20, 21) for in situ correction of most disease-causing mutations while preserving the physiological regulation of the targeted gene (22–26). Here, we developed and selected the best performing strategy to correct RAG1 deficiency targeting either intron 1 or exon 2 of *hRAG1* in human HSPCs. Our results support the implementation of the exonic gene editing (GE) strategy toward clinical application for the treatment of RAG1 deficiency.

RESULTS

Immune recovery in *Rag1*$^{-/-}$ mice with low dose of functional HSPCs

To model the therapeutic potential of HSPC GE, we took advantage of *Rag1*$^{-/-}$ mice, which recapitulate the human T-B-SCID (27). We performed competitive transplantations of wild-type (WT) and *Rag1*$^{-/-}$ HSPCs, admixed at different ratios, in total body irradiated *Rag1*$^{-/-}$ recipient mice to determine the minimal fraction of corrected cells required to rescue the immunological defects seen in these mice (Fig. 1A). We stratified transplanted mice into four experimental groups, based on the myeloid chimerism of donor WT cells in their peripheral blood, and compared them to WT untreated mice (WT untreated), and to *Rag1*$^{-/-}$ mice transplanted with either fully WT-HSPC (70–100% WT chimerism, positive controls) or fully *Rag1*$^{-/-}$-HSPC (100% KO, negative controls). As expected, all *Rag1*$^{-/-}$ mice treated with fully WT-HSPCs rescued white blood cell (WBC), T- and B-lymphocyte proportions and counts in parallel with reciprocal decrease in the proportion of myeloid cells (CD11b^{+}/B220^{-}CD19^{-}) in peripheral blood as compared to mice receiving KO cells (fig. S1, A and B). The redistribution of hematopoietic lineages also occurred in the groups

with the lowest doses of WT cells (0–5%). Of note, the frequency and counts of peripheral T cells approached values that were similar to those observed in WT mice; however, only marginal reconstitution of the B-cell compartment was observed, supporting the notion that in *Rag1*$^{-/-}$ mice a stronger competition occurs during B-cell differentiation in the bone marrow (BM) than among thymocytes, limiting the expansion and differentiation capacity of B-cell precursors (16). Granular analyses of T cell differentiation in the thymus indicated that 0–5% WT cells could overcome T cell development block in *Rag1*$^{-/-}$ mice, as shown by a decrease in the proportion of double negative (DN) $CD4^{-}CD8^{-}$ T cells and by progression of T cell differentiation through double positive (DP) $CD4^{+}CD8^{+}$ and single positive $CD4^{+}CD8^{-}$ and $CD8^{+}CD4^{-}$ cell stages as compared to what observed in *Rag1*$^{-/-}$ mice receiving KO cells. A statistically significant decrease in the proportion of DN cells was reached in *Rag1*$^{-/-}$ mice with >5% WT cells (p values vs 100% KO: 5–10% WT 0.035; 10–15% WT 0.0006; 70–100% WT <0.0001; Fig. 1B). These findings paralleled a significant increase of $CD4^{+}$ and $CD8^{+}$ T cell counts in the thymus (fig. S1C) and spleen (Fig. 1C and fig. S1D). Rescue of the proportion of naïve and effector/memory T cells was observed in the spleen of *Rag1*$^{-/-}$ mice transplanted with increasing doses of WT cells (fig. S1E), suggesting that the increased T-cell counts were not due to peripheral homeostatic proliferation. In the B-cell compartment, all mice engrafted with WT cells showed a significant increase of immature B cells in BM (p values vs 100% KO: 0–5% WT 0.0072; 5–10% WT 0.0007; 10–15% WT 0.001; 70–100% WT <0.0001; Fig. 1D), demonstrating that even a low WT-cell proportion could overcome the B-cell differentiation block. These data suggested that the peripheral B-cell lymphopenia (fig. S1B) was due to low B-cell output from the BM (fig. S1F), further corroborating the hypothesis of high cellular competition in BM. Nevertheless, *Rag1*$^{-/-}$ mice with low fractions of WT cells showed statistically significant improvement of B-cell counts in the spleen (p values *vs* 100% KO: 0–5% WT 0.0067; 5–10% WT 0.0006; Fig. 1E) encompassing all stages of B-cell maturation (Fig. S1G). in vivo B-cell function was demonstrated in terms of IgG, IgM and IgA production at steady state (Fig. 1F and fig. S1H) and specific Ig response upon in vivo T-cell dependent antigen immunization (fig. S1I). The decrease of B-cell activation factor (BAFF) concentration (Fig. 1G), a cytokine required for B-cell homeostasis and associated with autoimmunity when overexpressed (28), supported the normalization of B-cell compartment.

To more stringently mimic the rescue potential of cells bearing monoallelic editing, which conceivably represents the most frequent HDR outcome upon GE of HSPCs, we verified whether the transplant of low proportions of heterozygous *Rag*$^{+/-}$ (*Rag1*-HETERO) HSPCs rescued immune cell defects in *Rag1*$^{-/-}$ mice. The proportion of 0–5% of *Rag1*-HETERO allowed the improvement of WBC, T- and B-cell frequency and counts in peripheral blood (fig. S2, A and B). We observed a decrease in the proportion of DN cells in the thymus of *Rag1*$^{-/-}$ mice with 0–5% of *Rag1*-HETERO chimerism, and normalization in the distribution of differentiating T-cell subsets in *Rag1*$^{-/-}$ mice with ≥7–15% of *Rag1*-HETERO cells (Fig. 1H). These findings translated into increased proportions and counts of differentiated $CD4^{+}$ and $CD8^{+}$ T cells in thymus (fig. S2C) and spleen (Fig. 1I and fig. S2D) with naïve and effector/memory phenotypes (fig. S2E). The B-cell differentiation block was also overcome with more than 0–5% of *Rag1*-HETERO cells (Fig. 1J) and B-cell

counts in the BM improved as compared to *Rag1*$^{-/-}$ mice, although they did not reachthe values of positive controls (fig. S2F). Nevertheless, the presence of B cells in the spleen of *Rag1*$^{-/-}$ mice with 0–5% and 7–15% of *Rag1*-HETERO cells (Fig. 1K and fig. S2D) with proper peripheral maturation (fig. S2G) led to Ig production at steady state (Fig. 1L and fig. S2H) and after antigen challenge in vivo (fig. S2I) and was associated with decreased BAFF concentration (Fig. 1M).

Overall, low proportions of WT or *Rag1*-HETERO HSPCs improved the immune cell defects of *Rag1*-deficient mice, likely due to the strong selective advantage of properly maturing lymphocytes over their deficient counterparts, supporting the therapeutic potential of gene edited HSPCs.

hRAG1 editing by intronic knock-in

The human *RAG1* gene is composed of two exons, with exon 2 containing the whole coding sequence (5). We first designed a CRISPR/Cas9 GE strategy aimed at integrating a corrective *hRAG1* coding sequence into intron 1 to potentially correct any *hRAG1* mutation with clinical relevance by trapping the transcriptional activity of the endogenous promoter with a previously validated splice acceptor (SA) site (22, 26) (Fig. 2A). We screened a panel of nine guide RNAs (gRNAs) in NALM6-WT cells, a human pre-B cell line constitutively expressing *hRAG1*, selected the gRNA 9 as having the best on/off-target activity rofile (dig. S3, A to D and Tables S1 to S3), and validated its performance in human cord blood (CB) and mobilized peripheral blood (mPB) HSPCs upon delivery as preassembled gRNA/Cas9 ribonucleoproteins (RNPs) by electroporation (fig. S3E).

We then screened seven reporter constructs, all containing the splice acceptor (SA) sequence and homology arms for the gRNA 9 target site and each containing a different terminal sequence (SA-GFP constructs, fig. S3F) in NALM6-WT cells. The presence of an exogenous poly-adenylation site resulted in higher GFP expression compared to all other donors exploiting the *hRAG1* 3'UTR for transcriptional termination (fig. S3G), suggesting that the *hRAG1* 3'UTR negatively affects its expression. To evaluate regulation of transgene expression by the *hRAG1* promoter, edited NALM6-WT cells were deprived of serum supplementation (hereafter referred to as "serum starvation") to synchronize their cell cycle at G0/G1 phase when *hRAG1* gene was upregulated. Whereas all donors carrying or using the endogenous 3'UTR resulted in modulation of GFP expression upon starvation, this was not observed for the donor with exogenous polyA (fig. S3H). We thus selected the SA-co.hRAG1-BGHpA and the SA-co.hRAG1-SD for further testing upon incorporation into AAV6 donors carrying the corrective codon optimized *hRAG1* cDNA (co.hRAG1) (Fig. 2, A and B).

To assess the functionality of the different editing configurations of *hRAG1*, we generated a *hRAG1*-deficient NALM6 clonal cell line by Cas9 disruption confirmed in terms of RNA and protein expression (fig. S4, A to E). RAG1 recombination activity was then assessed by transducing bulk NALM6-WT cells and its single-cell-derived clone (E150) with LV carrying an inverted GFP (LV.PGK-iGFP) cassette flanked by the recombination signal sequences (RSS) specifically recognized by the hRAG1/RAG2 complex and followed by IRES-hCD4 as transduction marker (fig. S4F). If the RAG complex is functional, it will bind

the RSS and recombine the GFP cassette, which will be placed in the correct orientation resulting in GFP expression (29–32). Functional hRAG1 inactivation was confirmed in clone E150 (hereafter named NALM6-RAG1.KO) and its parental targeted population (fig. S4G).

NALM6-RAG1.KO cells were then treated with gRNA9/Cas9 RNP and either the SA-co.hRAG1-BGHpA or SA-co.hRAG1-SD AAV6 donor and their single-cell clonal outgrowths were screened for successful *hRAG1* editing by locus-specific ddPCR (Fig. 2C). Two out of 7 SA-co.hRAG1-BGHpA edited clones and 7 out of 12 SA-co.hRAG1-SD edited clones showed rescued recombination activity upon transduction with LV.PGK-iGFP as compared to unedited NALM6-RAG1.KO cells but with lower values than NALM6-WT cells (Fig. 2D and fig. S4H), suggesting suboptimal expression and/or regulation of the edited gene. Although co.hRAG1 mRNA was expressed in most edited clones, it was low and not modulated by starvation (Fig. 2E), different from the endogenous *hRAG1* expression in starved NALM6-WT cells (Fig. 2F).

Despite the incomplete rescue of expression, we decided to test the extent of functional correction achieved by these constructs in human HSPCs. We first optimized conditions for *hRAG1* intron 1 GE in CB and mPB-HSPCs (Fig. 2G) in terms of RNP and AAV6 doses, and co-delivered an mRNA encoding a dominant negative truncated p53 polypeptide (GSE56) (fig. S5, A to D) allowing transient inhibition of the p53-dependent DDR induced by DNA DSBs and AAV6 transduction (33, 34). When using the SA-co.hRAG1-BGHpA donor we achieved high proportions of targeted integration in bulk mPB-HSPCs from HDs (Fig. 2H), which lowered in the most primitive fraction (fig. S5E), as previously reported (22, 26, 34). Similar targeted integration was observed in mPB-HSPCs derived from two RAG1-deficient patients carrying hypomorphic *hRAG1* mutations and presenting with CID-G/AI (Fig. 2I). Although GE preserved the most primitive HSPCs and culture composition (Fig. 2, J and K), clonogenic assays showed reduced numbers of colonies as compared to untreated cells (Fig. 2L). To investigate the impact of GE on HD and patient HSPCs, we performed whole transcriptomic analysis of untreated and edited cells (fig. S5, F to H). Considering differentially regulated genes and pathways, we observed a higher activation status in hypomorphic RAG1-patients mPB-HSPCs induced by the culture manipulation, and the alleviation rather than full abrogation of the editing induced p53-dependent DNA damage response (DDR) by GSE56 (fig. S5, G and H).

To assess the engraftment potential and the multilineage repopulation capacity of gene edited HSPCs, we transplanted untreated and edited cells into NOD-SCID IL2Rγ null (NSG) mice.

Although RAG1-patient HSPCs resulted in lower engraftment as compared to HD-HSPCs, there was multilineage engraftment in all groups with no significant differences between edited and their unedited counterpart (Fig. 3, A and B), suggesting that the editing protocol did not substantially affect engraftment and repopulation capabilities. Although edited cells engrafted in the BM and spleen (fig. S6, A and B), no correction of lymphoid compartments was observed in mice transplanted with edited patient-HSPCs (Fig. 3, B to D), indicating that the intronic GE platform did not rescue the lymphoid defect.

For better characterization of T-cell differentiation after GE we exploited the artificial thymic organoid (ATO) platform (35). To improve HDR efficiency and to maximize the output of edited T cells from ATOs seeded with edited mPB-HSPCs, we also included in the GE protocol the adenoviral protein Ad5-E4orf6/7 to force cell-cycle progression and to upregulate components of HDR machinery (34, 36–39). The combination of the adenoviral protein Ad5-E4orf6/7 with GSE56 (COMBO) improved organoid morphology (fig. S6C), increased the number of viable cells (Fig. 3E), and improved the targeting efficiency yield of edited-ATO cells as compared to either GSE56 or Ad5-E4orf6/7 alone (Fig. 3F and fig. S6D). These findings were confirmed in mPB-HSPCs edited using the PGK-GFP-BGHpA donor, with an increase of HDR-efficiency in all T-cell subsets, especially in $CD3^{+}TCR\alpha/\beta^{+}$ cells (fig. S6, E and F). Next, we compared the SA-co.hRAG1-BGHpA and SA-co.hRAG1-SD AAV6 templates, using ATOs generated from HD and Pt_1-derived edited mPB-HSPCs. Although HDR efficiency in bulk and sorted T cells (Fig. 3G) was comparable and in line with that of HSPCs (Fig. 3H), edited patient's HSPCs remained mostly blocked at the DP stage, with lack of $CD3^{+}TCR\alpha/\beta^{+}$ T cells (Fig. 3I), ultimately showing insufficient expression and rescue of recombination activity from the intronic knock-in correction strategy.

Combined knock-out and knock-in by editing *hRAG1* exon 2

We speculated that preservation of the intronic sequence could be required for physiological gene regulation and set out to develop a strategy targeting the second *hRAG1* exon, which contains the entire coding sequence. We selected gRNA target sites to disrupt gene function to abrogate the interference or possible dominant negative effect of residual hypomorphic mutants on HDR corrected alleles (combined knock-out/knock-in strategy), and to further enhance the selective advantage of corrected cells over the others. We designed two corrective donors for each candidate target site that differed in the downstream configuration (Fig. 4, A and B). The "targeting" donor bore homology to both immediate sides of the DNA double strand break and the co.hRAG1 sequence would be inserted in-frame, leaving downstream the endogenous exon 2 sequence (Fig. 4A), whereas the "replacement" donor was conceived to favor excision of the downstream endogenous *hRAG1* sequences by recombining within the 3'UTR through a more distal but longer 3' homology arm (Fig. 4B).

To select gRNAs able to abolish endogenous *hRAG1* expression, we targeted nonstandard ATGs present at the N-terminus of *hRAG1* gene that might be engaged as alternative translation start sites resulting in truncated RAG1 with decreased recombination activity (40) (gRNAs g1ex to g6ex) (fig. S7A) in NALM6-WT cells. gRNA g6ex showed the highest cutting efficiency (fig. S7B), resulting in damping of *hRAG1* recombination activity (fig. S7, C and D). Functional correction of hRAG1 activity assessed in NALM6-RAG1.KO mono- and bi-allelic clones showed restoration of hRAG1 recombinase activity, reaching the proportion of GFP^{+} cells observed in untreated NALM6-WT cells at different time points of analysis (Fig. 4C and fig. S7E). Mono-allelic correction was sufficient to rescue hRAG1 function and its significantly increased expression upon starvation (Fig. 4C-D; p values vs bulk Rag1.KO: g6ex/Targ 0.0098; g6ex/Repl <0.0001; Fig. 4C; p values vs bulk Rag1.KO: g6ex/Targ 0.0078; g6ex/Repl 0.0312; Fig. 4D). However, the strategy resulted in low HDR efficiency in mPB-HSPCs, likely due to low nuclease activity (Fig. 4E). Thus, we selected 2

additional gRNAs (g11ex and g13ex) from a new panel targeting the same region (fig. S7A) and achieved more efficient targeting in HD-derived mPB-HSPCs (fig. S7F) with marked reduction of $CD3^+TCR\alpha/\beta^+$ T-cell frequency in ATOs (fig. S7G), confirming effective non-homologous or microhomology-mediated end joining (NH/MMEJ)-mediated *hRAG1* inactivation. Three-to-four-fold higher HDR efficiency was then documented in HD-derived mPB-HSPCs edited with g11ex or g13ex (Fig. 4H) instead of g6ex (Fig. 4E and fig. S7L).

We then assessed functional RAG1 correction in NALM6-RAG1.KO cells edited with g11ex or g13ex in combination with the targeting or replacement AAV6 donor. The increased recombination activity in bulk edited NALM6-RAG1.KO cells was in line with HDR values (fig. S7, H and I). Recombination activity in mono- and bi-allelic clones (fig. S7J) was significantly higher than untreated NALM6-RAG1.KO cells (Fig. 4F, p values vs bulk Rag1.KO: g11ex/Targ 0.0002, g11ex/Repl 0.0136, g13ex/Targ 0.0073, g13ex/Repl 0.0004; and fig. S7K) along with the modulation of co.hRAG1 expression upon starvation (Fig. 4G), confirming the robust correction potential of the exonic strategy.

In silico prediction of g11ex and g13ex off-targets returned high specificity scores and identified putative sites mostly in intronic or intergenic regions (fig. S8A and Tables S4 and S5). We complemented this analysis with a GUIDE-seq assay (41) using relaxed bioinformatic constraints to capture more potential off-target sites. GUIDE-seq detected two exonic and four intronic off-target sites for g11ex and only two intronic for g13ex (fig. S8A), indicating a more specific profile of g13ex (Fig. S8A and Table S6). Deep sequencing of g13ex off-targets was performed in three different mPB HD-derived HSPCs, edited with g13ex RNP alone and untreated (UT) as controls, confirming absent or very low nuclease activity at *in silico* predicted off-target sites and undetectable nuclease activity at off-targets sites nominated by GUIDE-seq analysis (fig. S8B and Table S7).

Rescue of hRAG1 in patient-derived HSPCs by editing exon 2

We tested our exonic GE strategy in Pt_1 mPB-HSPCs that could not be rescued with the intronic strategy. Both exon editing templates resulted in a high percentage of HDR-edited alleles in HD and patient-derived mPB-HSPCs, with a tendency to a higher proportion of edited alleles in g13ex-edited cells than g11ex-edited cells (Fig. 5A), in line with data on HD-HSPCs (Fig. 4K). GE preserved the most primitive $CD34^+CD133^+CD90^+$ fraction, especially in patient HSPCs (Fig. 5B). We then transplanted unedited and edited RAG1-patient-HSPCs in NSG mice, using g13ex alone due to constraints in availability of patient-derived HSPCs. Both HD- and Pt_1-derived HSPCs engrafted in NSG mice, with the latter showing a lower engraftment rate, improved at early time points for the edited cells (Fig. 5C). HDR-editing efficiency was high and stable in peripheral blood cells (fig. S9A). The frequency of B, T and myeloid cells was comparable among groups (Fig. 5D and fig. S9B), confirming that multilineage differentiation was not impaired by GE. The mouse transplanted with untreated patient cells showed low B-cell frequency when compared to HD-treated mice (Fig. 5D and fig. S9B), in line with the immune phenotype of patients carrying hypomorphic mutations (42). Both targeting and replacement strategies rescued peripheral B-cell frequencies in mice transplanted with edited patient HSPCs, with a kinetics of cell repopulation that was similar to that observed after transplantation of

HD cells (Fig. 5D and fig. S9B) explaining the improved graft size. The improved B-cell output in mice treated with edited patient-HSPCs was associated with reduced proportion of myeloid cells as compared to untreated patient-HSPCs transplant (Fig. 5D). Consistent with these observations, GE of *hRAG1* exon 2 allowed substantial improvement in the B-cell compartment in terms of frequencies and B-cell differentiation in the BM (Fig. 5, E and F). We observed a reduction of progenitor-B cell (Pro-B and Pre-B cells) subsets associated with the relative expansion of the last stages of B-cell development in mice treated with edited patient-HSPCs as compared to unedited cells (Fig. 5F). T-cell differentiation and output, which typically occur only at delayed times after transplant in this humanized model, were not affected by the editing procedure and the two corrective platforms in HD-grafted mice (Fig. 5D and fig. S9B). We observed a slight increase in T cells after editing of patient-HSPCs with the replacement donor (Fig. 5D and fig. S9B). However, the low or absent T-cell reconstitution in mice treated with edited patient HSPCs (Fig. 5D and fig. S9B) could be explained by the lower engraftment in BM of edited patient HSPCs as compared to HD-HSPCs (fig. S9, C and -D). Despite the low engraftment of edited RAG1-patient cells in the thymus (fig. S9, E and F), an increased proportion of $CD3^{+}TCR\alpha/\beta^{+}$ cells was observed in mice treated with edited patient-HSPCs as compared to mice with RAG1-mutated HSPCs (Fig. 5G).

Analysis of the kinetics of $CD3^{+}TCR\alpha/\beta^{+}$ cell generation in ATOs showed that g13ex RNP treatment fully blocked T-cell differentiation in HD cells (Fig. 5H and fig. S7G), which was restored by HDR when adding the corrective templates (Fig. 5H and fig. S9G), indicating the dual efficacy of the exonic knock-out/knock-in GE strategies. As expected and consistent with previously reported data (43), $CD34^{+}$ cells from patients carrying hypomorphic RAG mutations were unable to differentiate into $CD3^{+}TCR\alpha\beta^{+}$ cells in the ATO platform due to the missense *RAG1* mutations (Fig. 5I and fig. S9H). Both corrective donors were able to rescue hRAG1 function and overcome the T-cell differentiation block in edited patient cells when g13ex was used (Fig. 5I and fig. S9H), supporting the therapeutic potential of our exonic GE strategy. Molecular analysis of HDR efficiency in sorted T-cell subsets harvested from the ATOs showed higher proportions of edited alleles in g13ex-treated samples as compared to g11ex-treated samples (Fig. 5J), in line with the HDR values of input HSPCs (Fig. 5A).

To further investigate the robustness of T-cell development rescue, we analyzed the TCRβ repertoire of bulk or sorted $CD3^{+}TCR\alpha/\beta^{+}$ ATO cells by the high-throughput TCRB immunoSEQ assay. This analysis was not performed in UT RAG1 patients due to the absent $CD3^{+}TCR\alpha/\beta^{+}$ differentiation in the ATO platform (Fig. 3I, Fig. 4I and fig. S9H)(43). Hierarchical packcircle plots showed a similar diversity profile of TCRβ rearrangements between cells harvested from ATOs seeded with edited HD and RAG1-patient HSPCs (Fig. 5K), as confirmed by the Simpson Complexity index, a diversity metric measuring the sample clonality (Fig. 5L). Consistently, the productive entropy, corresponding to the Shannon's entropy, confirmed a greater number of rearrangements and little dominance by a subset of rearrangements in all tested samples (fig. S9I). we did observe a restricted repertoire in the case of HD-HSPCs electroporated with g13ex alone which was rescued by coadministration of the targeting and replacement donor templates (fig. S9J), in line with the

different impact on T cell output. Overall, our results support the therapeutic potential of the optimized exonic GE strategy for *in situ* genetic correction of human RAG1 deficiency.

Choice of IDLV as template delivery platform for exonic *hRAG1* gene editing

To support the clinical translation of GE and mitigate the adverse cellular impact and potential genotoxic risk associated to AAV6-mediated template delivery in HSPCs (44), we tested an optimized protocol exploiting integrase-defective lentiviral vector (IDLV). We cloned and manufactured IDLV targeting and replacement donors specific for g13ex target site and tested different doses, timings and rounds of IDLV transduction to select the best performing protocol, which was directly compared with the optimized AAV-based one. Cyclosporin H (CsH)-enhanced one hit IDLV transduction upon editing in presence of Ad5-E4orf6/7 and GSE56 (COMBO) was the best performing protocol for mPB HSPCs (Fig. 6A). A direct comparison between the optimized GE protocols using either AAV6- or IDLV-based template delivery showed similar HDR efficiency in bulk $CD34^+$ cells (Fig. 6B). Analysis of HSPC subpopulations showed a trend toward more efficient HDR editing in the most committed progenitors with AAV-based delivery, as previously reported (44). Of note, no difference was observed in the most primitive HSPCs (Fig. 6C), which were slightly better preserved upon IDLV than AAV6-based editing (Fig. 6D). Moreover, we observed a tendency to a more sustained HSPC clonogenic capacity with IDLV-mediated delivery (Fig. 6E). As performed above for the AAV6 delivery platform, hRAG1 functional rescue was tested after IDLV GE by exploiting the NALM6-RAG1.KO clones. Recombination activity assessed by LV.PGK-iGFP assay displayed higher frequency of GFP^+ cells in both IDLV targeting and replacement donors than untreated bulk KO cells (Fig. 6F). Furthermore, modulation of the co.hRAG1 expression after starvation was observed (Fig. 6G), indicating that the IDLV GE successfully rescued hRAG1 expression and function in KO edited clones. Taken together these data support that the IDLV platform can be a valuable alternative to AAV6-based GE and suggest its further development for the clinical translation of the exonic hRAG1 GE strategy.

DISCUSSION

Here, we developed an HDR-mediated GE strategy in human HSPCs that rescues physiologically regulated *hRAG1* expression and function, enabling V(D)J recombination during lymphopoiesis for the treatment of RAG1 deficiency. The proportion of corrected human HSPCs in mice xenotransplanted with edited HD or patient derived cells surpasses the lower threshold for correction of immune dysfunctions.

RAG gene defects lead to reduced survival and poor quality of life, unless treated by HSCT. However, HSCT outcome can be compromised by several factors including age, clinical status at the time of transplantation, donor availability, and transplant-related GvHD (3, 8, 11, 12). Autologous HSC gene therapy may thus provide an alternative treatment option. In an ongoing phase I/II clinical trial (NCT04797260) RAG1 SCID patients are being treated by HSC gene replacement therapy with an LV carrying the co.hRAG1 driven by the γRV-derived MND promoter and lacking the endogenous RAG1 3'UTR post-transcriptional regulation (14). However, the choice of a retroviral strong and constitutively active

promoter raises concerns for the long-term safety of this strategy, given the occurrence of myelodysplastic syndromes in adrenoleukodystrophy patients treated with an LV carrying the same promoter (https://www.fda.gov/media/159129/download). Moreover, constitutive expression of *hRAG1* cannot recapitulate physiological regulation, which could result in poor immune reconstitution and dysregulation (14, 18, 45), and potentially off-target RAG recombinase activity (46, 47). Instead, HDR-mediated GE offers the unique advantage of in situ editing the affected gene and preserving its physiological regulation (22, 24–26, 48, 49). We tailored 2D, 3D and in vivo tools to predict and validate the feasibility and efficacy of our platforms. We adapted the recombination assay and the ATO system to the GE platform, further expanding their application in the field of gene manipulation. Together with xenograft models, we exploited these tools to show that the exonic GE strategies outperformed the intronic one at the RAG1 locus, although we cannot exclude that selection of different intronic target sites may alleviate this disadvantage. Despite effective targeted integration of the corrective donor template and detectable expression of co.hRAG1, the intronic strategy might disrupt regulatory elements, reported in other first introns to control complex gene expression patterns (50, 51). Although intronic regulatory features mapping into *hRAG1* targeted region are currently unknown, a homozygous mutation in first intron of *hRAG1* caused lymphoid differentiation block and reduced *IgH* repertoire diversity (52). This evidence corroborates the hypothesis that the preservation of the intronic regulation of *hRAG1* is relevant for obtaining a functional rescue, as also demonstrated for X-CGD GE targeting the CYBB locus (53). At variance with the intronic strategy, the exonic targeting also maintains the proximity of the coding region to the endogenous 3’UTR, critical for post-transcriptional regulation (54). (49)Our data obtained from the screening of distinct corrective templates for intronic HDR-integration indicate that 3’UTR plays a role in the modulation of transgene expression. Thus, various regulation layers synergistically cooperating to stringently maintain proper *hRAG1* expression are preserved by our exonic GE platform.

A successful GE platform relies on the tailored selection of all reagents necessary to achieve substantial efficacy, specificity and predicted safety, while mitigating cytotoxicity and genotoxic risks, especially in the context of HSPCs which have self-renewal capacity. The selected gRNAs showed high specificity and a low risk profile based on off-target site analyses. However, deeper studies are needed to investigate genome integrity in an unbiased manner in gene edited HSPCs before moving to the clinical arena. Indeed, growing evidence shows that a relevant fraction of cells treated with editing nucleases may experience large deletions at the targeted locus, translocations, chromosomal arm loss and even chromotripsis (44, 55–58). Nevertheless, assessing genome integrity using PCR-based sequencing methods might introduce amplification artefacts and should be complemented by multimodal innovative platforms, such as optical genome mapping, long read sequencing and CAST-seq(59–61).

We exploited GSE56 and Ad5-E4orf6/7, which have been previously demonstrated to enhance HDR-editing efficiency in long-term HSPCs and to allow polyclonal composition of the human edited graft (34). Although inhibition of p53 may raise concerns for the acquisition of genomic rearrangements, the partial and transient nature of the inhibition alleviates this concern, and it may have the advantage of preventing selection of clones

bearing pre-existing or induced loss-of-function p53 mutations (62). It is likely that disease background factors, pharmacological treatments and disruption of BM niche (63),may account for the higher sensitivity to cell manipulation observed here for *hRAG1* mutated-HSPCs than HD cells and impacting on their clonogenic potential, transcriptomic profile and engraftment capability. The AAV6 vector platform was initially tested to deliver the donor repair cassette. However, increasing evidence has shown that the high burden of intact and fragmented AAV DNA triggers prolonged DNA damage response impacting the repopulation potential and graft clonal diversity in xenograft models(44, 64–67). Although AAVs has been considered a non-integrating platform, integration of inverted terminal repeats (ITRs) or full-length AAV DNA in on and off-target sites (44, 68–70) raised concerns for the possible impact of ITR transcription promoting activity on genes flanking insertions (44, 71–77). We moved to the IDLV platform and achieved in the most primitive HSPC subset similar HDR efficiency obtained with the AAV6 platform, indicating the feasibility and potential advantage of IDLV. Other protocols are emerging, such as lipid nanoparticles and prime editing to overcome the risk of viral sequence integration (78, 79), dsDNA and ssDNA as corrective donors, and base editing to target hot spot mutations (80, 81). Moreover, small molecules interfering with NHEJ-based repair could further enhance the target integration frequency (82) limiting the need for high IDLV multiplicity of infection (MOI).

Competitive transplant experiments showed that a threshold of >5–10% functional HSPCs provide benefits in *Rag1*$^{-/-}$ mice, especially in the T-cell lineage. B-cell reconstitution required higher donor chimerism, mirroring HSCT outcomes where patients often require prolonged immunoglobulin replacement therapy because B-cell reconstitution occurs later than other hematopoietic lineages (83). Our data indicated that a low proportion of WT/HETERO cells in *Rag1*$^{-/-}$ mice, engrafted upon conditioning, allowed long-term rescue of the secondary humoral response and argue in favour of including a conditioning regimen in HSCT-based therapies for RAG1 deficiency as recently indicated by the EBMT/ESID guidelines (9, 12, 84),(3, 16). Moreover, a stronger competition barrier is present in RAG1 hypomorphic conditions because of the additional presence of mutated mature T and B cells in periphery. For this reason, the exonic strategies were designed with the dual aim to dampen the competition exerted by host-derived lymphoid progenitors by exploiting NHEJ-mediated *hRAG1* disruption of the mutant endogenous *RAG1* gene and to *hRAG1* expression and function by HDR-mediated integration of a corrective copy of the gene. These strategies can enhance the potential of corrected HSPCs and, in turn, of their progeny to outperform mutant cells, thus effectively expanding the therapeutic application of exonic GE to hypomorphic *hRAG1* mutations. However, the complex scenario caused by the competition between residual hematopoiesis, *RAG1* HDR-edited and *RAG1* disrupted HSPCs has not been addressed in vivo. To further enhance the therapeutic advantage of gene edited HPSCs, we envisage combining autologous GE with biological conditioning that preserves non-hematopoietic tissues supportive for HSPC engraftment and fitness, and lymphoid maturation (22, 85–87), as we have previously shown in *Rag1* mouse models (13, 88).

There are several limitations to our study. Although we combined several tools to comprehensively demonstrate the efficacy of the exonic combined “knock-out and knock-in”

editing, the limited availability of RAG1 patient cells did not allow us to further investigate the biology and transcriptional profile of mutant RAG1 HSPCs after donor template delivery. As well, xenotransplant assays may not fully recapitulate all aspects of human RAG1 deficiency, although this is partially compensated by the competitive mouse-in-mouse transplant experiments.

Overall, we showed that HDR-editing of *hRAG1* exon 2 allows functional rescue of RAG1 defects by restoring its expression and activity, overcoming lymphoid differentiation block and leading to the generation of mature T and B cells. This study represents a proof-of-concept demonstration of therapeutically relevant HDR-correction of the *hRAG1* locus for the treatment of RAG1 deficiency, supporting further study of this exonic GE platform towards clinical testing.

MATERIALS AND METHODS

Study design

The goal of this study was to develop a GE strategy to functionally correct the *hRAG1* locus and treat RAG1 deficiency. Different panels of CRISPR/Cas9 nucleases and corrective donor templates were tested in HD and patient-derived HSPCs. Because of the limited availability of human HSPCs, especially those that were patient-derived, the sample size in each independent experiment was determined by the total number of available treated cells. To overcome this limitation, we generated a NALM6.Rag1-KO cell line to challenge all our platforms and assess the rescue of hRAG1 expression and function in terms of recombination activity. Moreover, we exploited the ATO system to use fewer HSPCs and assess their fitness and the ability of GE to overcome of the T-cell differentiation block. Each experiment was performed as independently as possible, on different days with different cell stocks, different batches of reagents and mouse litters. For all in vivo experiments, mice of similar age and sex were randomly assigned to experimental groups. Sample sizes were determined according to previous publications and experimental experience. All end points were prospectively determined by experimental design and each experiment was performed with sufficient power to detect effects. The investigators were blinded from the group allocation until the treatment and data collection were done. Experimental data were repeated to obtain an adequate number of biological replicates and the sample sizes, replicates, and statistics are reported in figures, figure legends, supplementary and data tables.

Mice and transplantation protocols

For competitive transplant experiments, C57Bl/6 wild-type (WT) mice were purchased from Charles River Laboratories Inc. (Calco, Italy). *B6.129S7-Rag.1*$^{t1Mom/J}$ mice (referred to as *Rag1*$^{-/-}$), purchased from The Jackson Laboratory, were maintained in specific pathogen-free (SPF) conditions (4 mice per cage) with 14-hour light/10-hour dark cycle or 12 light/12 dark cycle and a temperature of 65–75°F (~18–23°C) with 40–60% humidity following a normal diet of fat content ranges from 4% to 11%. *Rag1*$^{-/-}$ mice were mated to C57Bl/6 mice to generate *Rag*$^{+/-}$ mice. Lineage-negative (Lin^{-}) cells were isolated as described (89) from 6- to 10- weeks-old donor C57BL/6-CD45.1 WT or CD45.1/2 *Rag*$^{+/-}$ mice, mixed at

different ratios with CD45.2 *Rag1*$^{-/-}$ Lin^{-} cells, and intravenously transplanted at a total dose of 0.5×10^{6} cells into conditioned CD45.2 *Rag1*$^{-/-}$ mice (6–8 Gy total body irradiation).

For transplantation of human HSPCs, NOD-SCID IL2Rgnull mice (NSG) were purchased from Charles River Laboratories Inc and maintained in SPF conditions. Sublethally irradiated (180 cGy) 8–10 weeks-old NSG mice were transplanted with human CD34^{+} cells (0.4–1×10^{6}) at day +1 of the GE protocol (Fig. 2C). All animal procedures were performed with the approval of the Animal Care and Use Committee of the San Raffaele Hospital (Protocol 910 for competitive transplant experiments and Protocol 1129 for xenotransplantation in NSG mice) and communicated to the Ministry of Health and local authorities according to Italian law.

ELISA and in vivo immunization

Steady state plasma concentrations of total IgG, IgM, and IgA were measured 16 weeks after the transplant by using a multiplex assay (Beadlyte Mouse Immunoglobulin Isotyping kit, Millipore) on a Luminex Magpix instrument (Luminex Corp). B cell–activating factor (BAFF) concentrations were analyzed with the mouse BAFF Quantikine ELISA (R&D Systems), according to the manufacturer's instructions. In vivo challenge with the T-dependent antigen 2,4,6-trinitrophenyl (TNP)- conjugated keyhole limpet hemocyanin (TNP-KLH, Biosearch Technologies) and measurement of TNP-specific antibody titers were performed 16 weeks after transplantation as previously described (89).

Flow cytometry analyses

For analyses of competitive transplant experiments, single-cell suspensions were obtained from BM, spleen, thymus, and peripheral blood and stained with the mAbs listed in Table S8. Streptavidin phycoerythrin (PE)–cyanine 7 (Cy7) (BD PharMingen) was used for the detection of biotinylated antibody. For analyses of human HSPCs subpopulations and xenotransplant experiments with HSPCs, single-cell suspension was stained with the mAbs listed in Table S9. For the evaluation of hRAG1 recombination activity, GFP expression was analyzed on NALM6 cells collected 4 and 7 days upon starvation and stained with anti-human CD4 mAb (Table S9).

For all samples, LIVE/DEAD Fixable Yellow (ThermoFisher Scientific) or 7-aminoactinomycin (Sigma-Aldrich) was included in the sample preparation to exclude dead cells from the analysis according to the manufacturer's instructions. Sphero Rainbow Calibration Particles (Spherotech) beads were used to calibrate the instrument detectors for analysis performed at different time points. All samples were acquired on a FACSCanto II system (BD Biosciences, Calif) and analyzed with FlowJo software (TreeStar).

Cell lines and primary cell culture

K562, 293T, NALM6-WT (ATCC) and NALM6-RAG1.KO cell lines were cultured in RPMI 1640 medium (Corning) supplemented with 10% heat-inactivated fetal bovine serum (FBS) (Euroclone), 2mM L-glutamine (Euroclone) and 100U/I penicilin/streptomycin (Lonza). The murine stromal cell line (MS5) edited to ectopically express human Notch ligand, delta-like 4 (hDLL4) was used for ATO (35).

Human cord blood CD34$^+$ cells (CB-HSPCs) were obtained frozen from Lonza (PoieticsTM cat# 2C 101) and Granulocyte colony-stimulating factor (G-CSF) or G-CSF$^+$Plerixafor mPB CD34$^+$ (mPB-HSPCs) cells were purchased frozen from Lonza or purified in house with the CliniMACS CD34 Reagent System (Miltenyi Biotec) from Mobilized Leukopak (AllCells) according to the TIGET-HPCT protocol approved by OSR Ethical Committee and following the manufacturer's instructions. They were stimulated before GE at the concentration of 0.5×10^6 cells/ml in serum-free StemSpan™ SFEM (StemCell Technology) medium supplemented with specific early-acting cytokines (26, 34)

Patient mPB-CD34$^+$ cells were kindly provided by L.D. Notarangelo (Laboratory of Clinical Immunology and Microbiology, Division of Intramural Research, National Institute of Allergy and Infectious Diseases, National Institutes of Health,). Informed consent for biological samples' collection and anonymized biological sample/data sharing for RAG1 patients were obtained according to protocol NCT00001405 (www.clinicaltrials.gov), approved by the National Institutes of Health Institutional Review Board (IRB). RAG1-patient here named Pt_1 (NIHPID0021) is an adult male patient with CID-G/AI due to missense *RAG1* mutations (C1228T; G1520A), receiving anti-CD20 mAb treatment to control severe autoimmune manifestations. Pt_2 (NM_000448) is a 43 year-old male with compound heterozygous mutations (c.322C>T, p.R108X; c.1566G>T, p.W522), presenting with recurrent sinopulmonary infections, autoimmunity, and vocal cord granulomas. Both patients were under corticosteroid treatment. Peripheral blood-CD34$^+$ cells were isolated after mobilization with G-CSF and plerixafor. The experiments conformed to the principles set out in the WMA Declaration of Helsinki and the Department of Health and Human Services Belmont Report.

Nucleases and viral vectors

Sequences of the gRNAs were designed using CRISPOR online tool (http://crispor.tefor.net/) and selected for predicted specificity score and on-target activity. Ribonucleoproteins (RNPs) were assembled by incubating at a predefined 1:1.5 molar ratio Alt-R S.p. HiFi Cas9 Nuclease V3 protein (Integrated DNA Technologies) with synthetic two part gRNAs (cr:tracrRNA) (Integrated DNA Technologies) for 5 min at 95° and cool for 10 min at room temperature, or with synthetic single guide RNAs (sgRNAs) (Synthego) for 10 min at room temperature. Alt-R Electroporation Enhancer (Integrated DNA Technologies) was added prior to electroporation according to manufacturer's instructions, only when adding synthetic two-parts gRNAs from Integrated DNA Technologies. Guide RNA sequences are reported in the Table S10.

Donor construct maps were designed with SnapGene software v.6.0.2 (from GSL Biotech, available at snapgene.com). Plasmid for LV.PGK-iGFP was modified by substituting the GFP cDNA with the GFP.WPRE cassette from the pMX-RSS-GFP/IRES-hCD4 (pMX-INV) (29, 32) retroviral vector-based plasmid kindly provided by Prof. L.D. Notarangelo. Briefly, LVs were produced as previously described (90) by transient transfection of 293T cells with the transfer vector mixed with VSV-G envelope encoding plasmid, pMDLg/pRRE, REV plasmids and pADVANTAGE (Promega).

Plasmids carrying GFP cassette were generated in house by specific restriction enzyme (New England BioLabs) digestion and inserted into a dephosphorylated linearized backbone with either Quick Ligase or T4 Ligase after purification with QIAquick PCR Purification Kit (QIAGEN). After ligation, TOP10 chemically competent *E. Coli* bacteria were transformed and plated on plates containing antibiotics. Plasmid DNA was extracted and purified with Wizard Plus SV Minipreps DNA Purification System (Promega) and EndoFree Plasmid Maxi Kit (QIAGEN).

Donor Plasmid carrying the corrective *co.hRAG1* cDNA were synthetized by Genscript Biotech Corp. Lyophilized constructs were resuspended in water (0.4ug/ul) and transformed using One Shot™ TOP10 Chemically Competent E.coli cells. Plasmidic DNA was isolated using NucleoBond Xtra Maxi Endotoxin Free kit (Macherey-Nagel). AAV6 vectors were produced by the AAV Vector core at InnovaVector (TIGEM, Pozzuoli, Italy) by triple-transfection of HEK293 method and purification by ultracentrifugation with two rounds of cesium chloride gradient.

IDLV donors ware generated by the SR-Tiget Vector Core using HIV-derived, third-generation self-inactivating transfer constructs for the donor template, a D64V integrase mutant packaging construct and an HIV Rev and VSV.G expressing plasmids. IDLV stocks were prepared by transient transfection of HEK293T. At 30 hours post-transfection, vector-containing supernatants were collected, filtered, clarified, DNAse treated and loaded on a DEAE-packed column for Anion Exchange Chromatography. The vector-containing peaks were collected, subjected to a second round of DNAse treatment, concentration by Tangential Flow Filtration and a final Size Exclusion Chromatography separation followed by sterilizing filtration and titration of the purified stocks as previously described (90).

Gene editing on cell lines and primary cells

For GE on cell lines, after three days of culture, $0.5–1\times10^6$ cells were washed with Dulbecco's Phospate Buffered Saline (DPBS, Corning) and electroporated using SF Cell 4D-Nucleofector X Kit and Nucleofector 4D device (programs: NALM6, DS100; K562, FF120; 293T, Q-001; Lonza). Cells were electroporated with linearized nuclease plasmids or RNPs (at concentrations specified in the text) with Alt-R Electroporation Enhancer (Integrated DNA Technologies) only for two-parts gRNAs. Fifteen minutes after electroporation, cells were transduced with donor templates at indicated MOI.

For GE on human CB- or mPB-HSPCs we followed the previous described protocols (34). After three days of stimulation $0.2–0.7\times10^6$ cells were washed with DPBS and electroporated using P3 Primary Cell 4D-Nucleofector X Kit and Nucleofector device (program EO-100) (Lonza). Cells were electroporated with RNPs at indicated concentrations together with Alt-R Electroporation Enhancer (Integrated DNA Technologies) only for two-parts gRNAs. AAV6 transduction was performed 15 minutes after electroporation at the indicated doses. For 1-hit IDLV GE protocol, treatment with CsH (8μM) and transduction with IDLVs (MOI 150) were performed 15 min after electroporation. According to the experiments, 3 μg of GSE56 mRNA, 1.5 μg Ad5-E4orf6/7 mRNA or 5 μg of their combination as single RNA(34)were transfected along with RNP before AAV6 or IDLV transduction.

Recombination activity assay

NALM6-WT or NALM6-RAG1.KO cells transduced with LV.PGK-iGFP (MOI 5) and kept in culture in RPMI 1640 medium (Corning) supplemented with 10% heat-inactivated FBS (Euroclone), 2mM L-glutamine (Euroclone) and 100U/mL penicillin/streptomycin (Lonza). After six days cells were kept in serum starvation or treated with 4uM CDK4/6i (CalbioChem) to synchronize cell cycle phase in G1 phase when recombination activity is high. No differences were observed between the two starvation methods (fig. S7F). Flow cytometric analysis was performed after four and seven days of starvation: cells efficiently transduced were hCD4+ and only those cells with functional RAG1/2 complex were GFP^+. Four days after starvation, cells were collected for gene expression analyses.

Clonogenic assay

Colony-forming-unit cell (CFU-C) assay was performed by plating in three technical replicates 800 HSPCs/each in methylcellulose based medium (MethoCult, STEMCELL Technologies) supplemented with 100 IU/ml penicillin and 100μg/ml streptomycin. Two weeks after plating, colonies were counted and classified according to morphological criteria.

Artificial thymic organoids

The ATO platform is generated by aggregating a MS5-hDLL4 cell line (kindly provided by G.M. Crooks, Department of Pathology and Laboratory Medicine, David Geffen School of Medicine, Univ. of California, Los Angeles (UCLA)) with CB- or mPB-HSPCs, as previously described (35).

Molecular analyses

Indels induced by NHEJ were measured by a mismatched-sensitive endonuclease assay by PCR-based amplification of the targeted locus (as previously described (22, 34)) followed by digestion with T7 endonuclease I (T7E1, New England Biolabs) according to the manufacturer's instructions. Digested DNA fragments were resolved and quantified by capillary electrophoresis on LabChip® GX Touch HT (Perkin Elmer) or 4200 TapeStation System (Agilent) according to manufacturer's instructions. NHEJ efficiency was calculated as the ratio of the uncleaved parental fragment versus cleaved fragments.

For HDR digital droplet PCR (ddPCR) analysis, 15–10ng of genomic DNA were analyzed using the QX200 Droplet Digital PCR System (Bio-Rad) according to manufacturer's instructions. Primers and probes for ddPCR were designed on the junction between the targeted locus and the donor sequence. Human TTC5 (Bio-Rad) was used as normalizer. The percentage of cells harboring biallelic integration was calculated with the following formula: (concentration (copies/μl) of target+ droplets / concentration of TELO+ droplets) ×100.

Expression of the endogenous *hRAG1* or the exogenous co.hRAG1 was assessed on total RNA extracted using RNeasy Micro Kit (QIAGEN) according to manufacturer's instructions and retrotranscribed to cDNA using High-Capacity cDNA Reverse Transcription Kit (Applied Biosystems). 1–5ng of cDNA was then used for quantification by RT-qPCR using Power SYBR™ Green PCR Master Mix (Applied Biosystems). Human RPLPO and Beta-

actin were used as normalizers. Primers and probes sequences for NHEJ, HDR and gene expression are listed in Table S11.

RNA-seq

Whole transcriptomic analysis was performed on a pool of HSPCs derived from 2 mPB HDs and 2 RAG1 patients. Total RNA was isolated before the stimulation culture (d-3) and 24 hours after the editing (d+1) using miRNeasy Micro Kit (QIAGEN), and DNase treatment was performed using RNase-free DNase Set (QIAGEN), according to the manufacturer's instructions. Unedited cells (not electroporated and not transduced) collected at d+1 were used as comparative group for the edited cells at same time point. RNA samples passed quantity and quality criteria for library preparation and sequencing on a NextSeq 500 High 150 (Illumina). RNA-seq details and bioinformatic analysis are described in Supplementary Materials and Methods.

Western blot assay

Cellular proteins were extracted, separated by SDS-PAGE and transferred onto Trans-Blot Turbo Mini 0.2 μm Nitrocellulose Transfer Packs (BioRad) using the Trans-Blot Turbo Apparatus (BioRad). The following primary antibodies were used: anti-human RAG1 (1:500; Cell Signaling Technology– cat. #D36B3); anti-human p38 (1:2000 Cell Signaling Technology – cat. #9212); b-actin. Goat anti-rabbit IgG (1:2000; Cell Signaling Technology - cat. #7074) was used as secondary antibody conjugated to horseradish peroxidase (HRP). Immunostained bands were detected using the chemiluminescent method (ECL Prime Western Blotting Detection Regeants – Amersham™) and images were obtained by ChemiDoc Imaging Systems (BioRad).

Off-target analyses

In silico prediction of off-target profile was performed with CRISPOR (http://crispor.tefor.net). For GUIDE-seq analysis 1×10^6 K562 cells were electroporated with 50 pmol of High Fidelity Cas9 Nuclease V3 and a specific gRNA as RNP in presence of 200pmol dsODN (41). After editing with dsODN, cells were collected, and genomic DNA was extracted with QIAamp DNA Micro Kit (QIAGEN). Successful dsODN integration at the on-target site was evaluated by restriction fragment polymorphism assay using NdeI enzyme (NEB) and 4×10^6 viable cells were collected for library preparation and sequencing performed by Creative Biogen Biotechology using Unique Molecular Identifier (UMI) for tracking PCR duplicates. Quality checking and trimming were performed on the sequencing reads, using FastQC (v 0.11.9) and Trim_galore (v 0.6.6), respectively. High quality reads were aligned against the human reference genome (GRCh38), using Bowtie2 (v 2.3.5) (91) in the "very-sensitive-local" mode, in order to achieve optimal alignments. GUIDE-seq data analysis was performed employing the R/Bioconductor package GUIDE-seq (v.1.24.0) (92), and using UMI to deduplicate reads. To deepen the investigation to very weak potential off-targets, relaxed constraints (minimum number of 10 reads and maximum number of 10 mismatches) were applied. Visualization of off-target alignments were perfomed by Jalview cross-platform program (v 2.11.2.6, https://www.jalview.org) (93).

Deep sequencing and bioinformatic analysis

For amplicon deep sequencing, we generated amplicon libraries with two rounds of PCR (primers listed in Table S11) starting from >50–100 ng of purified gDNA from three independently edited and unedited HDs. The first PCR step was performed with GoTaq G2 Flexi DNA Polymerase (Promega) according to manufacturer instruction using the following amplification protocol: 95°C x 5'min, (95°C x 0.45 min, 60–65°C x 0.45 min, 72°C x 1 min) x 20 cycles, 72°C x 10min. The second PCR step was performed with GoTaq G2 Flexi DNA Polymerase (Promega) according to manufacturer instruction using 5 ul of the first-step PCR product and the following amplification protocol: 95°C x 5'min, (95°C x 0.45 min, 60–65°C x 0.45 min, 72°C x 1 min) x 20 cycles, 72°C x 10min. Second-step PCR was performed with primers containing sample specific barcodes and adaptors. PCR amplicons were then purified with Wizard SV Gel and PCR Clean-Up (Promega). Concentration and quality of amplicons were assessed by QuantiFluor ONE dsDNA system (Promega) and 4200 Tapestation System (Agilent). Amplicons from up to 100 differently tagged samples were multiplexed at equimolar ratios and run by Genewiz (Azenta Life Sciences) on HiSeq 2×150bp paired end sequencing (Illumina).

Sequencing analysis was performed by using CRISPResso2 (http://crispresso2.pinellolab.org/submission), a software tool for the evaluation and comparison of sequencing data from gene editing samples (94). We post-processed the CRISPResso2 outputs by comparing each sample with the corresponding UT control for the identification of indel events and excluded substitutions to reduce potential false positive outputs.

TCRB repertoire

TCR repertoire was analysed by a high-throughput and bias-controlled multiplex PCR amplification of TCR Beta sequence performed by immunoSEQ assay (Adaptive Biotechnology). Details are described in Supplementary Materials and Methods.

Statistical analyses

Inferential and modelling techniques were applied in presence of adequate sample sizes ($n \geq 5$), otherwise only descriptive statistics are reported. Due to the nature of collected variables, nonparametric inferential procedures have been implemented: the Mann-Whitney test was performed to compare two independent groups, Wilcoxon matched-pairs test was used for paired comparisons; whereas in presence of more than two independent groups the Kruskal-Wallis test followed by post-hoc analysis using Dunn's test was used. The false discovery rate (FDR) approach was used to adjust p-values for multiplicity. To analyze the kinetics of cell reconstitution over time, random-intercept linear mixed-effects (LME) models (95) were fitted, including a mouse specific random-effect term and results are shown in Table S12. When fitting LME models, standard transformations (logarithm, square/cubic root, ordered quantile normalization) were applied to outcome variables in order to satisfy model assumptions. Post-hoc analysis after LME was performed to examine all the pairwise comparisons between treatment groups at a fixed time point. Once more, FDR procedure was used as method for adjusting p-values.

Analyses were performed using GraphPad Prism v.9.4.0 (GraphPad) and R statistical software (version 4.1.2, https://cran.r-project.org/index.html). Values are expressed as Mean ± SEM and *P* values are showed as: *≤0.05; **≤0.01; ***≤0.001; ****≤0.0001.

Supplementary Material

Refer to Web version on PubMed Central for supplementary material.

Acknowledgments:

We thank the San Raffaele Flow Cytometry facility (Fractal) and the Center for Omics Sciences; A. Auricchio and M. Doria (TIGEM and InnovaVector, Naples) for AAV6 production; and C. Di Serio for coordinating CUSSB (Vita-Salute San Raffaele University). Some schematics shown in fig 2 and fig. 4 were created using www.BioRender.com.

Funding:

Telethon Foundation TIGET Core Grant E2 (A. Villa), and TIGET Core Grant E4 (LN); Italian Ministry of University and Research grant PRIN 2017 Prot. 20175XHBPN (A. Villa, LN); E-rare3 JTC2017 program, grant EDSCIDPROG (LN); National Institutes of Health grant R01AI155796 (PG); Division of Intramural Research, National Institute of Allergy and Infectious Diseases, National Institutes of Health, grant AI001222 (LDN).This work was partially supported by GeneSpire, a biotechnology startup developing LV-based liver gene transfer and hematopoietic cell gene editing. C. Brandas and D. Canarutto conducted this study as partial fulfilment of their PhD (Translational and Molecular Medicine-DIMET, Milano-Bicocca University; Molecular Medicine, International Ph.D. School, Vita-Salute San Raffaele University; Milan, Italy, respectively).

Data and materials availability:

All data associated with this study are available in the paper or the supplementary materials and data files. RNA-seq, off-target and targeted deep-sequencing data have been deposited at GEO and are publicly available under the accession number GSE244753. Material transfer agreements were signed with Prof. Luigi D. Notarangelo (NIAID) for human mPB-HSPCs from patients with RAG1 deficiency, and with Prof. Gay M. Crooks (UCLA) for the MS5 cell line.

REFERENCES AND NOTES

1. Schatz DG, Swanson PC, V(D)J Recombination: Mechanisms of Initiation. Annu Rev Genet 45, 167–202 (2011). [PubMed: 21854230]
2. Dvorak CC, Haddad E, Heimall J, Dunn E, Cowan MJ, Pai S-Y, Kapoor N, Satter LF, Buckley RH, O'Reilly RJ, Chandra S, Bednarski JJ, Williams O, Rayes A, Moore TB, Ebens CL, Davila Saldana BJ, Petrovic A, Chellapandian D, Cuvelier GDE, vander Lugt MT, Caywood EH, Chandrakasan S, Eissa H, Goldman FD, Shereck E, Aquino VM, Desantes KB, Madden LM, Miller HK, Yu L, Broglie L, Gillio A, Shah AJ, Knutsen AP, Andolina JP, Joshi AY, Szabolcs P, Kapadia M, Martinez CA, Parrot RE, Sullivan KE, Prockop SE, Abraham RS, Thakar MS, Leiding JW, Kohn DB, Pulsipher MA, Griffith LM, Notarangelo LD, Puck JM, The diagnosis of severe combined immunodeficiency: Implementation of the PIDTC 2022 Definitions. Journal of Allergy and Clinical Immunology 151, 547–555.e5 (2023). [PubMed: 36456360]
3. Villa A, Notarangelo LD, RAG gene defects at the verge of immunodeficiency and immune dysregulation. Immunol Rev 287, 73–90 (2019). [PubMed: 30565244]
4. Delmonte OM, Schuetz C, Notarangelo LD, RAG Deficiency: Two Genes, Many Diseases. J Clin Immunol 38, 646–655 (2018). [PubMed: 30046960]
5. Notarangelo LD, Kim M-S, Walter JE, Lee YN, Human RAG mutations: biochemistry and clinical implications. Nat Rev Immunol 16, 234 (2016). [PubMed: 26996199]

6. Schuetz C, Huck K, Gudowius S, Megahed M, Feyen O, Hubner B, Schneider DT, Manfras B, Pannicke U, Willemze R, Knüchel R, Göbel U, Schulz A, Borkhardt A, Friedrich W, Schwarz K, Niehues T, An immunodeficiency disease with RAG mutations and granulomas. New England Journal of Medicine 358, 2030–2038 (2008). [PubMed: 18463379]
7. Dvorak CC, Haddad E, Buckley RH, Cowan MJ, Logan B, Griffith LM, Kohn DB, Pai S-Y, Notarangelo L, Shearer W, Prockop S, Kapoor N, Heimall J, Chaudhury S, Shyr D, Chandra S, Cuvelier G, Moore T, Shenoy S, Goldman F, Smith AR, Sunkersett G, Vander Lugt M, Caywood E, Quigg T, Torgerson T, Chandrakasan S, Craddock J, Dávila Saldaña BJ, Gillio A, Shereck E, Aquino V, DeSantes K, Knutsen A, Thakar M, Yu L, Puck JM, The genetic landscape of severe combined immunodeficiency in the United States and Canada in the current era (2010–2018). Journal of Allergy and Clinical Immunology 143, 405–407 (2019). [PubMed: 30193840]
8. Lankester AC, Neven B, Mahlaoui N, von Asmuth EGJ, Courteille V, Alligon M, Albert MH, Serra IB, Bader P, Balashov D, Beier R, Bertrand Y, Blanche S, Bordon V, Bredius RG, Cant A, Cavazzana M, Diaz-de-Heredia C, Dogu F, Ehlert K, Entz-Werle N, Fasth A, Ferrua F, Ferster A, Formankova R, Friedrich W, Gonzalez-Vicent M, Gozdzik J, Güngör T, Hoenig M, Ikinciogullari A, Kalwak K, Kansoy S, Kupesiz A, Lanfranchi A, Lindemans CA, Meisel R, Michel G, Miranda NAA, Moraleda J, Moshous D, Pichler H, Rao K, Sedlacek P, Slatter M, Soncini E, Speckmann C, Sundin M, Toren A, Vettenranta K, Worth A, Yeşilipek MA, Zecca M, Porta F, Schulz A, Veys P, Fischer A, Gennery AR, Hematopoietic cell transplantation in severe combined immunodeficiency: The SCETIDE 2006–2014 European cohort. Journal of Allergy and Clinical Immunology 149, 1744–1754.e8 (2022). [PubMed: 34718043]
9. Haddad E, Logan BR, Griffith LM, Buckley RH, Parrott RE, Prockop SE, Small TN, Chaisson J, Dvorak CC, Murnane M, Kapoor N, Abdel-Azim H, Hanson IC, Martinez C, Bleesing JJH, Chandra S, Smith AR, Cavanaugh ME, Jyonouchi S, Sullivan KE, Burroughs L, Skoda-Smith S, Haight AE, Tumlin AG, Quigg TC, Taylor C, Dávila Saldaña BJ, Keller MD, Seroogy CM, Desantes KB, Petrovic A, Leiding JW, Shyr DC, Decaluwe H, Teira P, Gillio AP, Knutsen AP, Moore TB, Kletzel M, Craddock JA, Aquino V, Davis JH, Yu LC, Cuvelier GDE, Bednarski JJ, Goldman FD, Kang EM, Shereck E, Porteus MH, Connelly JA, Fleisher TA, Malech HL, Shearer WT, Szabolcs P, Thakar MS, vander Lugt MT, Heimall J, Yin Z, Pulsipher MA, Pai S-Y, Kohn DB, Puck JM, Cowan MJ, R. J. O'Reilly, Notarangelo LD, SCID genotype and 6-month posttransplant CD4 count predict survival and immune recovery. Blood 132, 1737–1749 (2018). [PubMed: 30154114]
10. Ciurea SO, Bittencourt MCB, Milton DR, Cao K, Kongtim P, Rondon G, Chen J, Konopleva M, Perez JMR, el Shazly MF, Aljadayeh M, Alvarez M, Im J, Al-Atrash G, Mehta R, Popat U, Bashir Q, Oran B, Hosing CM, Khouri IF, Kebriaei P, Champlin RE, Is a matched unrelated donor search needed for all allogeneic transplant candidates? Blood Adv 2, 2254–2261 (2018). [PubMed: 30206098]
11. Schuetz C, Gerke J, Ege M, Walter J, Kusters M, Worth A, Kanakry JA, Dimitrova D, Wolska-Kuśnierz B, Chen K, Unal E, Karakukcu M, Pashchenko O, Leiding J, Kawai T, Amrolia PJ, Berghuis D, Buechner J, Buchbinder D, Cowan MJ, Gennery AR, Güngör T, Heimall J, Miano M, Meyts I, Morris EC, Rivière J, Sharapova SO, Shaw PJ, Slatter M, Honig M, Veys P, Fischer A, Cavazzana M, Moshous D, Schulz A, Albert MH, Puck JM, Lankester AC, Notarangelo LD, Neven B, Hypomorphic RAG deficiency: impact of disease burden on survival and thymic recovery argues for early diagnosis and HSCT. Blood 141, 713–724 (2023). [PubMed: 36279417]
12. Schuetz C, Neven B, Dvorak CC, Leroy S, Ege MJ, Pannicke U, Schwarz K, Schulz AS, Hoenig M, Sparber-Sauer M, Gatz SA, Denzer C, Blanche S, Moshous D, Picard C, Horn BN, de Villartay J-P, Cavazzana M, Debatin K-M, Friedrich W, Fischer A, Cowan MJ, SCID patients with ARTEMIS vs RAG deficiencies following HCT: increased risk of late toxicity in ARTEMIS-deficient SCID. Blood 123, 281–289 (2014). [PubMed: 24144642]
13. Villa A, Capo V, Castiello MC, Innovative Cell-Based Therapies and Conditioning to Cure RAG Deficiency. Front Immunol 11 (2020), doi:10.3389/fimmu.2020.607926.
14. Garcia-Perez L, van Eggermond M, van Roon L, Vloemans SA, Cordes M, Schambach A, Rothe M, Berghuis D, Lagresle-Peyrou C, Cavazzana M, Zhang F, Thrasher AJ, Salvatori D, Meij P, Villa A, van Dongen JJM, Zwaginga J-J, van der Burg M, Gaspar HB, Lankester A, Staal FJT, Pike-Overzet K, Successful Preclinical Development of Gene Therapy for Recombinase-Activating Gene-1-Deficient SCID. Mol Ther Methods Clin Dev 17, 666–682 (2020). [PubMed: 32322605]

15. Pike-Overzet K, Rodijk M, Ng YY, Baert MRM, Lagresle-Peyrou C, Schambach A, Zhang F, Hoeben RC, Hacein-Bey-Abina S, Lankester AC, Bredius RGM, Driessen GJA, Thrasher AJ, Baum C, Cavazzana-Calvo M, van Dongen JJM, Staal FJT, Correction of murine Rag1 deficiency by self-inactivating lentiviral vector-mediated gene transfer. Leukemia 25, 1471–1483 (2011). [PubMed: 21617701]

16. Lagresle-Peyrou C, Yates F, Malassis-Séris M, Hue C, Morillon E, Garrigue A, Liu A, Hajdari P, Stockholm D, Danos O, Lemercier B, Gougeon ML, Rieux-Laucat F, de Villartay JP, Fischer A, Cavazzana-Calvo M, Long-term immune reconstitution in RAG-1-deficient mice treated by retroviral gene therapy: A balance between efficiency and toxicity. Blood 107, 63–72 (2006). [PubMed: 16174758]

17. Charrier S, Lagresle-Peyrou C, Poletti V, Rothe M, Cédrone G, Gjata B, Mavilio F, Fischer A, Schambach A, de Villartay J-P, Cavazzana M, Hacein-Bey-Abina S, Galy A, Biosafety Studies of a Clinically Applicable Lentiviral Vector for the Gene Therapy of Artemis-SCID. Mol Ther Methods Clin Dev 15, 232–245 (2019). [PubMed: 31720302]

18. van Til NP, Sarwari R, Visser TP, Hauer J, Lagresle-Peyrou C, van der Velden G, Malshetty V, Cortes P, Jollet A, Danos O, Cassani B, Zhang F, Thrasher AJ, Fontana E, Poliani PL, Cavazzana M, Verstegen MMA, Villa A, Wagemaker G, Recombination-activating gene 1 (Rag1)–deficient mice with severe combined immunodeficiency treated with lentiviral gene therapy demonstrate autoimmune Omenn-like syndrome. Journal of Allergy and Clinical Immunology 133, 1116–1123 (2014). [PubMed: 24332219]

19. van Til NP, Cortes P, Danos O, Cassani B, Poliani PL, Villa A, Wagemaker G, Reply. Journal of Allergy and Clinical Immunology 134, 243–244 (2014). [PubMed: 25117804]

20. Doudna JA, The promise and challenge of therapeutic genome editing. Nature 578, 229–236 (2020). [PubMed: 32051598]

21. Scully R, Panday A, Elango R, Willis NA, DNA double-strand break repair-pathway choice in somatic mammalian cells. Nat Rev Mol Cell Biol 20, 698–714 (2019). [PubMed: 31263220]

22. Schiroli G, Ferrari S, Conway A, Jacob A, Capo V, Albano L, Plati T, Castiello MC, Sanvito F, Gennery AR, Bovolenta C, Palchaudhuri R, Scadden DT, Holmes MC, Villa A, Sitia G, Lombardo A, Genovese P, Naldini L, Preclinical modeling highlights the therapeutic potential of hematopoietic stem cell gene editing for correction of SCID-X1. Sci Transl Med 9 (2017), doi:10.1126/scitranslmed.aan0820.

23. Dever DP, Bak RO, Reinisch A, Camarena J, Washington G, Nicolas CE, Pavel-Dinu M, Saxena N, Wilkens AB, Mantri S, Uchida N, Hendel A, Narla A, Majeti R, Weinberg KI, Porteus MH, CRISPR/Cas9 β-globin gene targeting in human haematopoietic stem cells. Nature 539, 384–389 (2016). [PubMed: 27820943]

24. Rai R, Romito M, Rivers E, Turchiano G, Blattner G, Vetharoy W, Ladon D, Andrieux G, Zhang F, Zinicola M, Leon-Rico D, Santilli G, Thrasher AJ, Cavazza A, Targeted gene correction of human hematopoietic stem cells for the treatment of Wiskott - Aldrich Syndrome. Nat Commun 11, 4034 (2020). [PubMed: 32788576]

25. de Ravin SS, Li L, Wu X, Choi U, Allen C, Koontz S, Lee J, Theobald-Whiting N, Chu J, Garofalo M, Sweeney C, Kardava L, Moir S, Viley A, Natarajan P, Su L, Kuhns D, Zarember KA, Peshwa M. v., Malech HL, CRISPR-Cas9 gene repair of hematopoietic stem cells from patients with X-linked chronic granulomatous disease. Sci Transl Med 9 (2017), doi:10.1126/scitranslmed.aah3480.

26. Vavassori V, Mercuri E, Marcovecchio GE, Castiello MC, Schiroli G, Albano L, Margulies C, Buquicchio F, Fontana E, Beretta S, Merelli I, Cappelleri A, Rancoita PM, Lougaris V, Plebani A, Kanariou M, Lankester A, Ferrua F, Scanziani E, Cotta-Ramusino C, Villa A, Naldini L, Genovese P, Modeling, optimization, and comparable efficacy of T cell and hematopoietic stem cell gene editing for treating hyper-IgM syndrome. EMBO Mol Med 13 (2021), doi:10.15252/emmm.202013545.

27. Mombaerts P, Iacomini J, Johnson RS, Herrup K, Tonegawa S, Papaioannou VE, RAG-1-deficient mice have no mature B and T lymphocytes. Cell 68, 869–877 (1992). [PubMed: 1547488]

28. Schweighoffer E, Tybulewicz VL, BAFF signaling in health and disease. Curr Opin Immunol 71, 124–131 (2021). [PubMed: 34352467]

29. Liang H-E, Hsu L-Y, Cado D, Cowell LG, Kelsoe G, Schlissel MS, The “Dispensable” Portion of RAG2 Is Necessary for Efficient V-to-DJ Rearrangement during B and T Cell Development. Immunity 17, 639–651 (2002). [PubMed: 12433370]
30. Bredemeyer AL, Sharma GG, Huang C-Y, Helmink BA, Walker LM, Khor KC, Nuskey B, Sullivan KE, Pandita TK, Bassing CH, Sleckman BP, ATM stabilizes DNA double-strand-break complexes during V(D)J recombination. Nature 442, 466–470 (2006). [PubMed: 16799570]
31. De Ravin SS, Cowen EW, Zarember KA, Whiting-Theobald NL, Kuhns DB, Sandler NG, Douek DC, Pittaluga S, Poliani PL, Lee YN, Notarangelo LD, Wang L, Alt FW, Kang EM, Milner JD, Niemela JE, Fontana-Penn M, Sinal SH, Malech HL, Hypomorphic Rag mutations can cause destructive midline granulomatous disease. Blood 116, 1263–1271 (2010). [PubMed: 20489056]
32. Lee YN, Frugoni F, Dobbs K, Walter JE, Giliani S, Gennery AR, Al-Herz W, Haddad E, LeDeist F, Bleesing JH, Henderson LA, Pai S-Y, Nelson RP, El-Ghoneimy DH, El-Feky RA, Reda SM, Hossny E, Soler-Palacin P, Fuleihan RL, Patel NC, Massaad MJ, Geha RS, Puck JM, Palma P, Cancrini C, Chen K, Vihinen M, Alt FW, Notarangelo LD, A systematic analysis of recombination activity and genotype-phenotype correlation in human recombination-activating gene 1 deficiency. Journal of Allergy and Clinical Immunology 133, 1099–1108.e12 (2014). [PubMed: 24290284]
33. Schiroli G, Conti A, Ferrari S, della Volpe L, Jacob A, Albano L, Beretta S, Calabria A, Vavassori V, Gasparini P, Salataj E, Ndiaye-Lobry D, Brombin C, Chaumeil J, Montini E, Merelli I, Genovese P, Naldini L, Di Micco R, Precise Gene Editing Preserves Hematopoietic Stem Cell Function following Transient p53-Mediated DNA Damage Response. Cell Stem Cell 24, 551–565.e8 (2019). [PubMed: 30905619]
34. Ferrari S, Jacob A, Beretta S, Unali G, Albano L, Vavassori V, Cittaro D, Lazarevic D, Brombin C, Cugnata F, Kajaste-Rudnitski A, Merelli I, Genovese P, Naldini L, Efficient gene editing of human long-term hematopoietic stem cells validated by clonal tracking. Nat Biotechnol 38, 1298–1308 (2020). [PubMed: 32601433]
35. Seet CS, He C, Bethune MT, Li S, Chick B, Gschweng EH, Zhu Y, Kim K, Kohn DB, Baltimore D, Crooks GM, Montel-Hagen A, Generation of mature T cells from human hematopoietic stem and progenitor cells in artificial thymic organoids. Nat Methods 14, 521–530 (2017). [PubMed: 28369043]
36. Seandel M, Butler JM, Kobayashi H, Hooper AT, White IA, Zhang F, Vertes EL, Kobayashi M, Zhang Y, Shmelkov S. v., Hackett NR, Rabbany S, Boyer JL, Rafii S, Generation of a functional and durable vascular niche by the adenoviral *E4ORF1* gene. Proceedings of the National Academy of Sciences 105, 19288–19293 (2008).
37. Frese KK, Lee SS, Thomas DL, Latorre IJ, Weiss RS, Glaunsinger BA, Javier RT, Selective PDZ protein-dependent stimulation of phosphatidylinositol 3-kinase by the adenovirus E4-ORF1 oncoprotein. Oncogene 22, 710–721 (2003). [PubMed: 12569363]
38. Javier RT, Rice AP, Emerging Theme: Cellular PDZ Proteins as Common Targets of Pathogenic Viruses. J Virol 85, 11544–11556 (2011). [PubMed: 21775458]
39. Huang MM, Hearing P, The adenovirus early region 4 open reading frame 6/7 protein regulates the DNA binding activity of the cellular transcription factor, E2F, through a direct complex. Genes Dev 3, 1699–1710 (1989). [PubMed: 2532611]
40. Santagata S, Gomez CA, Sobacchi C, Bozzi F, Abinun M, Pasic S, Cortes P, Vezzoni P, Villa A, N-terminal RAG1 frameshift mutations in Omenn’s syndrome: Internal methionine usage leads to partial V(D)J recombination activity and reveals a fundamental role in vivo for the N-terminal domains. Proceedings of the National Academy of Sciences 97, 14572–14577 (2000).
41. Tsai SQ, Zheng Z, Nguyen NT, Liebers M, Topkar V. v., Thapar V, Wyvekens N, Khayter C, Iafrate AJ, Le LP, Aryee MJ, Joung JK, Ved V, Thapar V, Wyvekens N, Khayter C, Iafrate AJ, Le P, Aryee MJ, Joung JK, Unit P, Hospital MG, Hospital MG, Institutet K, GUIDE-Seq enables genome-wide profiling of off. Nat Biotechnol 33, 187–197 (2015). [PubMed: 25513782]
42. Delmonte OM, Villa A, Notarangelo LD, Immune dysregulation in patients with RAG deficiency and other forms of combined immune deficiency. Blood 135, 610–619 (2020). [PubMed: 31942628]
43. Bosticardo M, Pala F, Calzoni E, Delmonte OM, Dobbs K, Gardner CL, Sacchetti N, Kawai T, Garabedian EK, Draper D, Bergerson JRE, DeRavin SS, Freeman AF, Güngör T, Hartog N, Holland SM, Kohn DB, Malech HL, Markert ML, Weinacht KG, Villa A, Seet CS, Montel-Hagen

A, Crooks GM, Notarangelo LD, Artificial thymic organoids represent a reliable tool to study T-cell differentiation in patients with severe T-cell lymphopenia. Blood Adv 4, 2611–2616 (2020). [PubMed: 32556283]

44. Ferrari S, Jacob A, Cesana D, Laugel M, Beretta S, Varesi A, Unali G, Conti A, Canarutto D, Albano L, Calabria A, Vavassori V, Cipriani C, Castiello MC, Esposito S, Brombin C, Cugnata F, Adjali O, Ayuso E, Merelli I, Villa A, Di Micco R, Kajaste-Rudnitski A, Montini E, Penaud-Budloo M, Naldini L, Choice of template delivery mitigates the genotoxic risk and adverse impact of editing in human hematopoietic stem cells. Cell Stem Cell 29, 1428–1444.e9 (2022). [PubMed: 36206730]
45. Pike-Overzet K, Baum C, Bredius RGM, Cavazzana M, Driessen G-J, Fibbe WE, Gaspar HB, Hoeben RC, Lagresle-Peyrou C, Lankester A, Meij P, Schambach A, Thrasher A, van Dongen JJM, Zwaginga J-J, Staal FJT, Successful RAG1-SCID gene therapy depends on the level of RAG1 expression. Journal of Allergy and Clinical Immunology 134, 242–243 (2014). [PubMed: 25117803]
46. Teng G, Maman Y, Resch W, Kim M, Yamane A, Qian J, Kieffer-Kwon K-R, Mandal M, Ji Y, Meffre E, Clark MR, Cowell LG, Casellas R, Schatz DG, RAG Represents a Widespread Threat to the Lymphocyte Genome. Cell 162, 751–765 (2015). [PubMed: 26234156]
47. Papaemmanuil E, Rapado I, Li Y, Potter NE, Wedge DC, Tubio J, Alexandrov LB, Van Loo P, Cooke SL, Marshall J, Martincorena I, Hinton J, Gundem G, Van Delft FW, Nik-Zainal S, Jones DR, Ramakrishna M, Titley I, Stebbings L, Leroy C, Menzies A, Gamble J, Robinson B, Mudie L, Raine K, O'meara S, Teague JW, Butler AP, Cazzaniga G, Biondi A, Zuna J, Kempski H, Muschen M, Ford AM, Stratton MR, Greaves M, Campbell PJ, RAG-mediated recombination is the predominant driver of oncogenic rearrangement in ETV6-RUNX1 acute lymphoblastic leukemia. Nat Genet 46, 116–125 (2014). [PubMed: 24413735]
48. Gardner CL, Pavel-Dinu M, Dobbs K, Bosticardo M, Reardon PK, Lack J, DeRavin SS, Le K, Bello E, Pala F, Delmonte OM, Malech H, Montel-Hagan A, Crooks G, Acuto O, Porteus MH, Notarangelo LD, Gene Editing Rescues In vitro T Cell Development of RAG2-Deficient Induced Pluripotent Stem Cells in an Artificial Thymic Organoid System. J Clin Immunol 41, 852–862 (2021). [PubMed: 33650026]
49. Iancu O, Allen D, Knop O, Zehavi Y, Breier D, Arbiv A, Lev A, Lee YN, Beider K, Nagler A, Somech R, Hendel A, Multiplex HDR for disease and correction modeling of SCID by CRISPR genome editing in human HSPCs. Mol Ther Nucleic Acids 31, 105–121 (2023). [PubMed: 36618262]
50. Rose AB, Introns as Gene Regulators: A Brick on the Accelerator. Front Genet 9 (2019), doi:10.3389/fgene.2018.00672.
51. Park SG, Hannenhalli S, Choi SS, Conservation in first introns is positively associated with the number of exons within genes and the presence of regulatory epigenetic signals. BMC Genomics 15, 526 (2014). [PubMed: 24964727]
52. Min Q, Meng X, Zhou Q, Wang Y, Li Y, Lai N, Xiong E, Wang W, Yasuda S, Yu M, Zhang H, Sun J, Wang X, Wang J-Y, RAG1 splicing mutation causes enhanced B cell differentiation and autoantibody production. JCI Insight 6 (2021), doi:10.1172/jci.insight.148887.
53. Sweeney CL, Zou J, Choi U, Merling RK, Liu A, Bodansky A, Burkett S, Kim J-W, de Ravin SS, Malech HL, Targeted Repair of CYBB in X-CGD iPSCs Requires Retention of Intronic Sequences for Expression and Functional Correction. Molecular Therapy 25, 321–330 (2017). [PubMed: 28153086]
54. Mayr C, What Are 3′ UTRs Doing? Cold Spring Harb Perspect Biol 11, a034728 (2019). [PubMed: 30181377]
55. Adikusuma F, Piltz S, Corbett MA, Turvey M, McColl SR, Helbig KJ, Beard MR, Hughes J, Pomerantz RT, Thomas PQ, Large deletions induced by Cas9 cleavage. Nature 2018 560:7717 560, E8–E9 (2018).
56. V Zuccaro M, Xu J, Mitchell C, Lobo R, Treff N, Correspondence DE, Allele-Specific Chromosome Removal after Cas9 Cleavage in Human Embryos. Cell 183, 1650–1664 (2020). [PubMed: 33125898]

57. Leibowitz ML, Papathanasiou S, Doerfler PA, Blaine LJ, Sun L, Yao Y, Zhang CZ, Weiss MJ, Pellman D, Chromothripsis as an on-target consequence of CRISPR–Cas9 genome editing. Nat Genet 53, 895–905 (2021). [PubMed: 33846636]
58. Madi A, Ben-David U, Barzel A, Frequent aneuploidy in primary human T cells after CRISPR–Cas9 cleavage. Nat Biotechnol 40, 1807–1815 (2022). [PubMed: 35773341]
59. Turchiano G, Andrieux G, Klermund J, Blattner G, Pennucci V, el Gaz M, Monaco G, Poddar S, Mussolino C, Cornu TI, Boerries M, Cathomen T, Quantitative evaluation of chromosomal rearrangements in gene-edited human stem cells by CAST-Seq. Cell Stem Cell 28, 1136–1147.e5 (2021). [PubMed: 33626327]
60. Tsai H-H, Kao H-J, Kuo M-W, Lin C-H, Chang C-M, Chen Y-Y, Chen H-H, Kwok P-Y, Yu AL, Yu J, Whole genomic analysis reveals atypical non-homologous off-target large structural variants induced by CRISPR-Cas9-mediated genome editing. Nat Commun 14, 5183 (2023). [PubMed: 37626063]
61. Ferrari S, Valeri E, Conti A, Scala S, Aprile A, Di Micco R, Kajaste-Rudnitski A, Montini E, Ferrari G, Aiuti A, Naldini L, Genetic engineering meets hematopoietic stem cell biology for next-generation gene therapy. Cell Stem Cell 30, 549–570 (2023). [PubMed: 37146580]
62. Enache OM, Rendo V, Abdusamad M, Lam D, Davison D, Pal S, Currimjee N, Hess J, Pantel S, Nag A, Thorner AR, Doench JG, Vazquez F, Beroukhim R, Golub TR, Ben-David U, Cas9 activates the p53 pathway and selects for p53-inactivating mutations. Nat Genet 52, 662–668 (2020). [PubMed: 32424350]
63. Mitroulis I, Kalafati L, Bornhäuser M, Hajishengallis G, Chavakis T, Regulation of the Bone Marrow Niche by Inflammation. Front Immunol 11, 1540 (2020). [PubMed: 32849521]
64. Pattabhi S, Lotti SN, Berger MP, Singh S, Lux CT, Jacoby K, Lee C, Negre O, Scharenberg AM, Rawlings DJ, In Vivo Outcome of Homology-Directed Repair at the HBB Gene in HSC Using Alternative Donor Template Delivery Methods. Molecular Therapy of Nucleic Acids 17, 277–288 (2019). [PubMed: 31279229]
65. Pavani G, Laurent M, Fabiano A, Cantelli E, Sakkal A, Corre G, Lenting PJ, Concordet J-P, Toueille M, Miccio A, Amendola M, Ex vivo editing of human hematopoietic stem cells for erythroid expression of therapeutic proteins. Nat Commun 11 (2020), doi:10.1038/s41467-020-17552-3.
66. Schiroli G, Conti A, Ferrari S, della Volpe L, Jacob A, Albano L, Beretta S, Calabria A, Vavassori V, Gasparini P, Salataj E, Ndiaye-Lobry D, Brombin C, Chaumeil J, Montini E, Merelli I, Genovese P, Naldini L, Di Micco R, Precise Gene Editing Preserves Hematopoietic Stem Cell Function following Transient p53-Mediated DNA Damage Response. Cell Stem Cell 24, 551–565.e8 (2019). [PubMed: 30905619]
67. Romero Z, Lomova A, Said S, Miggelbrink A, Kuo CY, Campo-Fernandez B, Hoban MD, Masiuk KE, Clark DN, Long J, Sanchez JM, Velez M, Miyahira E, Zhang R, Brown D, Wang X, Kurmangaliyev YZ, Hollis RP, Kohn DB, Editing the Sickle Cell Disease Mutation in Human Hematopoietic Stem Cells: Comparison of Endonucleases and Homologous Donor Templates. Molecular therapy 27, 1389–1406 (2019). [PubMed: 31178391]
68. Hanlon KS, Meltzer JC, Buzhdygan T, Cheng MJ, Sena-Esteves M, Bennett RE, Sullivan TP, Razmpour R, Gong Y, Ng C, Nammour J, Maiz D, Dujardin S, Ramirez SH, Hudry E, Maguire CA, Selection of an Efficient AAV Vector for Robust CNS Transgene Expression. Mol Ther Methods Clin Dev 15, 320–332 (2019). [PubMed: 31788496]
69. Nelson CE, Wu Y, Gemberling MP, Oliver ML, Waller MA, Bohning JD, Robinson-Hamm JN, Bulaklak K, Castellanos Rivera RM, Collier JH, Asokan A, Gersbach CA, Long-term evaluation of AAV-CRISPR genome editing for Duchenne muscular dystrophy. Nature Medicine 2019 25:3 25, 427–432 (2019).
70. Cesana D, Calabria A, Rudilosso L, Gallina P, Benedicenti F, Spinozzi G, Schiroli G, Magnani A, Acquati S, Fumagalli F, Calbi V, Witzel M, Bushman FD, Cantore A, Genovese P, Klein C, Fischer A, Cavazzana M, Six E, Aiuti A, Naldini L, Montini E, Retrieval of vector integration sites from cell-free DNA. Nat Med 27, 1458–1470 (2021). [PubMed: 34140705]
71. Earley J, Piletska E, Ronzitti G, Piletsky S, Evading and overcoming AAV neutralization in gene therapy. (2022), doi:10.1016/j.tibtech.2022.11.006.

72. Keiser MS, Ranum PT, Yrigollen CM, Carrell EM, Smith GR, Muehlmatt AL, Chen YH, Stein JM, Wolf RL, Radaelli E, Lucas TJ, Gonzalez-Alegre P, Davidson BL, Toxicity after AAV delivery of RNAi expression constructs into nonhuman primate brain. Nat Med 27, 1982–1989 (2021). [PubMed: 34663988]
73. Ferrari S, Valeri E, Conti A, Scala S, Aprile A, Di Micco R, Kajaste-Rudnitski A, Montini E, Ferrari G, Aiuti A, Naldini L, Genetic engineering meets hematopoietic stem cell biology for next-generation gene therapy. Cell Stem Cell 30, 549–570 (2023). [PubMed: 37146580]
74. Colella P, Ronzitti G, Mingozzi F, Emerging Issues in AAV-Mediated In Vivo Gene Therapy. Mol Ther Methods Clin Dev 8 (2018), doi:10.1016/j.omtm.2017.11.007.
75. Dalwadi DA, Calabria A, Tiyaboonchai A, Posey J, Naugler WE, Montini E, Grompe M, AAV integration in human hepatocytes. Molecular Therapy 29, 2898–2909 (2021). [PubMed: 34461297]
76. Nguyen GN, Everett JK, A long-term study of AAV gene therapy in dogs with hemophilia A identifies clonal expansions of transduced liver cells. Nat Biotechnol 39, 47–55 (2021). [PubMed: 33199875]
77. Chandler RJ, Sands MS, Venditti CP, Recombinant Adeno-Associated Viral Integration and Genotoxicity: Insights from Animal Models. Hum Gene Ther 28, 314–322 (2017). [PubMed: 28293963]
78. Vavassori V, Ferrari S, Beretta S, Asperti C, Albano L, Annoni A, Gaddoni C, Varesi A, Soldi M, Cuomo A, Bonaldi T, Radrizzani M, Merelli I, Naldini L, Lipid nanoparticles allow efficient and harmless ex vivo gene editing of human hematopoietic cells. Blood 142, 812–826 (2023). [PubMed: 37294917]
79. Fiumara M, Ferrari S, Omer-Javed A, Beretta S, Albano L, Canarutto D, Varesi A, Gaddoni C, Brombin C, Cugnata F, Zonari E, Naldini MM, Barcella M, Gentner B, Merelli I, Naldini L, Genotoxic effects of base and prime editing in human hematopoietic stem cells. Nat Biotechnol (2023), doi:10.1038/s41587-023-01915-4.
80. McAuley GE, Yiu G, Chang PC, Newby GA, Campo-Fernandez B, Fitz-Gibbon ST, Wu X, Kang S-HL, Garibay A, Butler J, Christian V, Wong RL, Everette KA, Azzun A, Gelfer H, Seet CS, Narendran A, Murguia-Favela L, Romero Z, Wright N, Liu DR, Crooks GM, Kohn DB, Human T cell generation is restored in CD3δ severe combined immunodeficiency through adenine base editing. Cell 186, 1398–1416.e23 (2023). [PubMed: 36944331]
81. Liao J, Chen S, Hsiao S, Jiang Y, Yang Y, Zhang Y, Wang X, Lai Y, Bauer DE, Wu Y, Therapeutic adenine base editing of human hematopoietic stem cells. Nat Commun 14 (2023), doi:10.1038/s41467-022-35508-7.
82. Selvaraj S, Feist WN, Viel S, Vaidyanathan S, Dudek AM, Gastou M, Rockwood SJ, Ekman FK, Oseghale AR, Xu L, Pavel-Dinu M, Luna SE, Cromer MK, Sayana R, Gomez-Ospina N, Porteus MH, High-efficiency transgene integration by homology-directed repair in human primary cells using DNA-PKcs inhibition. Nat Biotechnol (2023), doi:10.1038/s41587-023-01888-4.
83. van der Maas NG, Berghuis D, van der Burg M, Lankester AC, B Cell Reconstitution and Influencing Factors After Hematopoietic Stem Cell Transplantation in Children. Front Immunol 10 (2019), doi:10.3389/fimmu.2019.00782.
84. Lankester AC, Albert MH, Booth C, Gennery AR, Güngör T, Hönig M, Morris EC, Moshous D, Neven B, Schulz A, Slatter M, Veys P, EBMT/ESID inborn errors working party guidelines for hematopoietic stem cell transplantation for inborn errors of immunity. Bone Marrow Transplant 56, 2052–2062 (2021). [PubMed: 34226669]
85. Palchaudhuri R, Saez B, Hoggatt J, Schajnovitz A, Sykes DB, Tate TA, Czechowicz A, Kfoury Y, Ruchika FNU, Rossi DJ, Verdine GL, Mansour MK, Scadden DT, Non-genotoxic conditioning for hematopoietic stem cell transplantation using a hematopoietic-cell-specific internalizing immunotoxin. Nat Biotechnol 34, 738–745 (2016). [PubMed: 27272386]
86. Pearse BR, McDonough SM, Proctor JL, Panwar R, Sarma G, McShea MA, Kien L, Dushime J, Adams HL, Hyzy SL, Brooks ML, Palchaudhuri R, Li Q, Kallen NM, Sawant P, McDonagh CF, Boitano AE, Cooke MP, CD117-Amanitin Antibody Drug Conjugates Effectively Deplete Human and Non-Human Primate HSCs: Proof of Concept As a Targeted Strategy for Conditioning Patients for Bone Marrow Transplant. Blood 132, 3314–3314 (2018).

87. Tisdale JF, Donahue RE, Uchida N, Pearse BR, McDonough SM, Proctor JL, Krouse A, Linde NS, Bonifacino AC, Panwar R, Sarma GN, Kien L, Latimer K, Dushime J, Hyzy SL, Brooks ML, Palchaudhuri R, Li Q, Sawant P, McDonagh CF, Boitano AE, Cooke MP, A Single Dose of CD117 Antibody Drug Conjugate Enables Autologous Gene-Modified Hematopoietic Stem Cell Transplant (Gene Therapy) in Nonhuman Primates. Blood 134, 610–610 (2019).

88. Castiello MC, Bosticardo M, Sacchetti N, Calzoni E, Fontana E, Yamazaki Y, Draghici E, Corsino C, Bortolomai I, Sereni L, Yu H-H, Uva P, Palchaudhuri R, Scadden DT, Villa A, Notarangelo LD, Efficacy and safety of anti-CD45–saporin as conditioning agent for RAG deficiency. Journal of Allergy and Clinical Immunology 147, 309–320.e6 (2021). [PubMed: 32387109]

89. Capo V, Castiello MC, Fontana E, Penna S, Bosticardo M, Draghici E, Poliani LP, Sergi Sergi L, Rigoni R, Cassani B, Zanussi M, Carrera P, Uva P, Dobbs K, Sacchetti N, Notarangelo LD, van Til NP, Wagemaker G, Villa A, Efficacy of lentivirus-mediated gene therapy in an Omenn syndrome recombination-activating gene 2 mouse model is not hindered by inflammation and immune dysregulation. Journal of Allergy and Clinical Immunology 142, 928–941.e8 (2018). [PubMed: 29241731]

90. Soldi M, Sergi Sergi L, Unali G, Kerzel T, Cuccovillo I, Capasso P, Annoni A, Biffi M, Rancoita PMV, Cantore A, Lombardo A, Naldini L, Squadrito ML, Kajaste-Rudnitski A, Laboratory-Scale Lentiviral Vector Production and Purification for Enhanced Ex Vivo and In Vivo Genetic Engineering. Mol Ther Methods Clin Dev 19, 411–425 (2020). [PubMed: 33294490]

91. Langmead B, Salzberg SL, Fast gapped-read alignment with Bowtie 2. Nat Methods 9, 357–359 (2012). [PubMed: 22388286]

92. Zhu LJ, Lawrence M, Gupta A, Pagès H, Kucukural A, Garber M, Wolfe SA, GUIDEseq: a bioconductor package to analyze GUIDE-Seq datasets for CRISPR-Cas nucleases. BMC Genomics 18, 379 (2017). [PubMed: 28506212]

93. Waterhouse AM, Procter JB, Martin DMA, Clamp M, Barton GJ, Jalview Version 2-a multiple sequence alignment editor and analysis workbench. Bioinformatics 25, 1189–1191 (2009). [PubMed: 19151095]

94. Clement K, Rees H, Canver MC, Gehrke JM, Farouni R, Hsu JY, Cole MA, Liu DR, Joung JK, Bauer DE, Pinello L, CRISPResso2 provides accurate and rapid genome editing sequence analysis. Nat Biotechnol 37, 224–226 (2019). [PubMed: 30809026]

95. Pinheiro J, Bates D, DebRoy S, Sarkar D, the R. C. Team, The nlme Package: Linear and Nonlinear Mixed Effects Models. R-project (2007).

96. Dobin A, Davis CA, Schlesinger F, Drenkow J, Zaleski C, Jha S, Batut P, Chaisson M, Gingeras TR, STAR: ultrafast universal RNA-seq aligner. Bioinformatics 29, 15–21 (2013). [PubMed: 23104886]

97. Liao Y, Smyth GK, Shi W, featureCounts: an efficient general purpose program for assigning sequence reads to genomic features. Bioinformatics 30, 923–930 (2014). [PubMed: 24227677]

98. Robinson Mark D, McCarthy Davis J, Smyth Gordon K, edgeR: a Bioconductor package for differential expression analysis of digital gene expression data. Bioinformatics 26 (2010).

99. Yu G, Wang L-G, Han Y, He Q-Y, clusterProfiler: an R Package for Comparing Biological Themes Among Gene Clusters. OMICS 16, 284–287 (2012). [PubMed: 22455463]

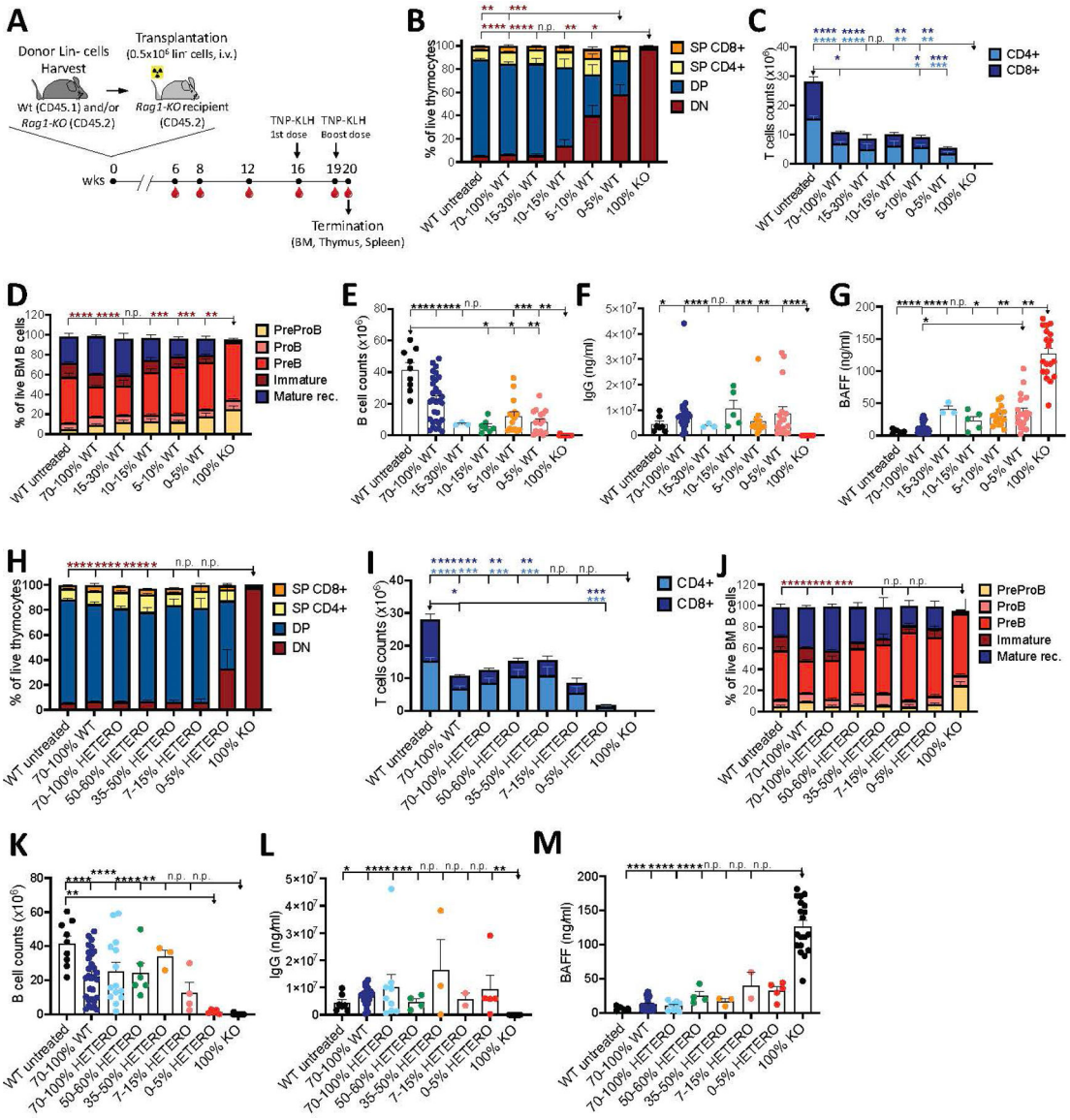

Figure 1. Immune reconstitution in competitive transplant experiments

A. Schematics\ of competitive transplant of CD45.1 WT Lineage negative (Lin$^-$) cells admixed at different ratio with CD45.2 *Rag1*$^{-/-}$ (*Rag1-KO*) cells in conditioned *Rag1-KO* mice. Immune reconstitution was assessed over time in peripheral blood and at termination by collecting bone marrow (BM), thymus and spleen. In vivo T-cell dependent response was evaluated by TNP-KHL challenge. **B.** Live double-negative (DN) CD4$^-$CD8$^-$, double-positive (DP) CD4$^+$CD8$^+$, single positive (SP) CD4$^+$CD8$^-$ and CD8$^+$CD4$^-$ cells were analyzed at termination by flow cytometry and shown as proportion of live thymocytes (WT untreated n=10; 70–100% WT n=32; 15–30% WT n=4; 10–15% WT n=7; 5–10% WT n=14; 0–5% WT n=18; 100% KO n=20). **C.** Splenic CD3$^+$CD4$^+$ and CD3$^+$CD8$^+$ T-cell counts are shown (WT untreated n=7; 70–100% WT n=30; 15–30% WT n=4; 10–15% WT n=7; 5–10% WT n=14; 0–5% WT n=17; 100% KO n=9). **D.** B-cell differentiation was analyzed by flow cytometry and shown as proportion of live BM B cells according

to the following immunophenotype: PreProB cells B220+CD43^{+}CD24^{-}, ProB cells B220^{+}CD43^{+}CD24^{+}, PreB cells B220^{+}CD43^{-}IgM^{-}, Immature cells B220^{+}CD43^{-}IgM^{hi}, Mature recirculant cells (Mature rec.) B220^{hi}CD43^{-}IgM$^{int/high}$ (WT untreated n=10; 70–100% WT n=33; 15–30% WT n=4; 10–15% WT n=7; 5–10% WT n=15; 0–5% WT n=19; 100% KO n=24). **E.** Splenic B-cell counts. **F-G.** Immunoglobulin G (IgG, **F**) and B-cell activating factor (BAFF, **G**) concentrations were analyzed in plasma 16 weeks after the transplant. **H.** Thymopoiesis in *Rag1-KO* mice transplanted with CD45.1/2 *Rag*$^{+/-}$ (HETERO) Lin- cells admixed at different ratio with CD45.2 KO Lin^{-} cells (WT untreated n=10; 70–100% WT n=32; 70–100% HETERO n=14; 50–60% HETERO n=5; 35–50% HETERO n=2; 7–15% HETERO n=4; 0–5% HETERO n=5; 100% KO n=20). **I.** Splenic CD4^{+} and CD8^{+} T-cell counts in *Rag1-KO* mice transplanted with HETERO Lin^{-} cells (WT untreated n=10; 70–100% WT n=30; 70–100% HETERO n=14; 50–60% HETERO n=6; 35–50% HETERO n=3; 7–15% HETERO n=4; 0–5% HETERO n=5; 100% KO n=9). **J.** B-cell differentiation in BM of *Rag1-KO* mice transplanted with HETERO Lin^{-} cells (WT untreated n=10; 70–100% WT n=30; 70–100% HETERO n=14; 50–60% HETERO n=6; 35–50% HETERO n=3; 7–15% HETERO n=4; 0–5% HETERO n=5; 100% KO n=24). **K.** Splenic B-cell counts in *Rag1-KO* mice transplanted with HETERO Lin^{-} cells. **L and M.** Immunoglobulin G (IgG, **L**) and B-cell activating factor (BAFF, **M**) concentrations were analyzed in plasma of *Rag1-KO* mice transplanted with HETERO Lin^{-} cells 16 weeks after the transplant. **B-M.** One-way ANOVA, Kruskal-Wallis test was used to assess statistically significant differences; asterisks were colored according to the legend; n.p., statistical analysis not performed when sample size was <5; arrows at the end of bars indicate the group to which all comparisons are statistically significant. *P* values are showed as: *≤0.05; **≤0.01; ***≤0.001; ****≤0.0001.

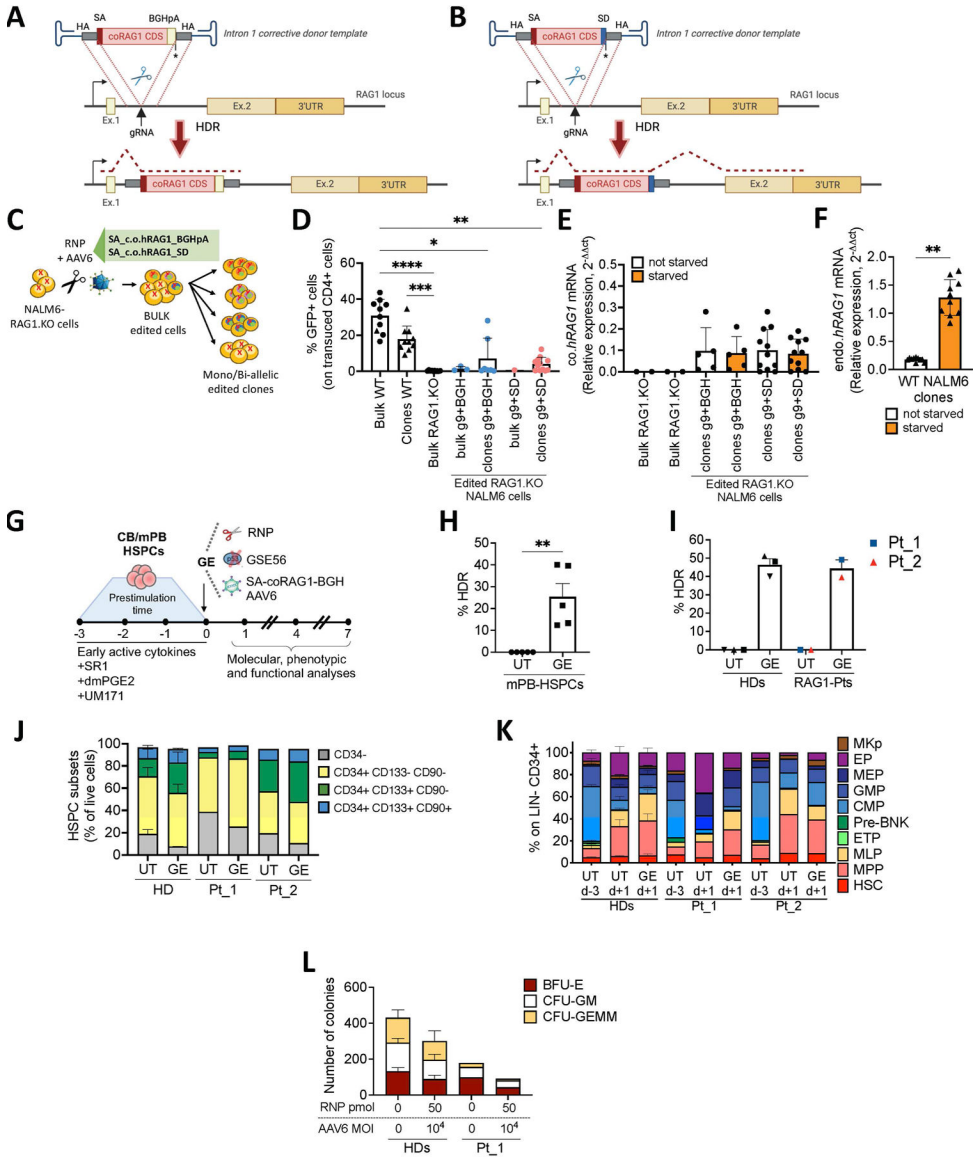

Figure 2. Development and impact of intronic gene editing strategies on human HSPCs

A and B. Schematics of GE strategies exploiting the *hRAG1* intronic target site and two distinct corrective donor templates: the SA-co.hRAG1-BGHpA, including the polyA sequence derived from Bovine Growth Hormone gene (BGH) (**A**), and the SA-co.hRAG1-SD which allows the use of the endogenous 3' UTR sequence (**B**). Panels were created using www.BioRender.com. **C.** Schematic of the GE protocol in NALM6-RAG1.KO cells edited by gRNA 9 and SA-co.hRAG1-BGHpA or SA-co.hRAG1-SD AAV6 donor. Bulk edited cells were single-cell sorted and mono- and bi-allelic edited clones were identified by ddPCR. **D.** RAG1 recombination activity was measured as proportion of GFP^+ cells gated on transduced $CD4^+$ cells in edited and unedited NALM6 cells (as bulk and single clones) assessed 7 days after serum-starvation by flow cytometry. One-way ANOVA, Kruskal-Wallis test was used to assess statistically significant differences. **E and F.** Expression of co.hRAG1 CDS in edited NALM6-RAG1.KO clones and controls

(unedited bulk NALM6-RAG1.KO cells) (**E**) and endogenous *hRAG1* in unedited NALM6-WT cells (**F**) were assessed 4 days after serum-starvation. Wilcoxon matched-pair test was used to assess statistically significant differences. **G.** Schematic of the GE protocol in human HSPCs. **H.** Percentage of HDR-edited alleles in untreated (UT) and gene edited (GE) HD mPB-HSPCs measured by ddPCR 4 days after editing. Mann-Whitney test was used to assess statistically significant differences. **I.** Percentage of HDR-edited alleles was measured by ddPCR 4 days after editing in untreated (UT) and gene edited (GE) mPB-HSPCs derived from HDs and patients with RAG1 deficiency (RAG1-PTs). **J.** Analysis of culture composition of mPB-HSPCs derived from HDs (n=3) and patient cells was performed by flow-cytometry four days after editing. **K.** Multiparametric dissection analysis of HSPC composition was performed before the prestimulation phase (d-3) and 1 day after the GE procedure (d+1) in unedited (UT) and edited (GE) cells. Graphs show 20 subtypes analysed in the Lineage negative (Lin^-) $CD34^+$ gate including: hematopoietic stem cells (HSC), multipotent progenitors (MPP), multi-lymphoid progenitors (MLP), early T progenitors (ETP), B and NK cell precursors (Pre-B/NK), common myeloid progenitors (CMP), granulocyte-monocyte progenitors (GMP), megakaryo-erythroid progenitors (MEP), megakaryocyte progenitors (MKp) and erythroid progenitors (EP). **L.** Number of colonies belonging to erythroid burst forming units (BFU-E), granulocyte-macrophage colony forming units (CFU-GM), and granulocyte, erythroid, macrophage, megakaryocyte units (CFU-GEMM). *P* values are showed as: *≤0.05; **≤0.01; ***≤0.001; ****≤0.0001.

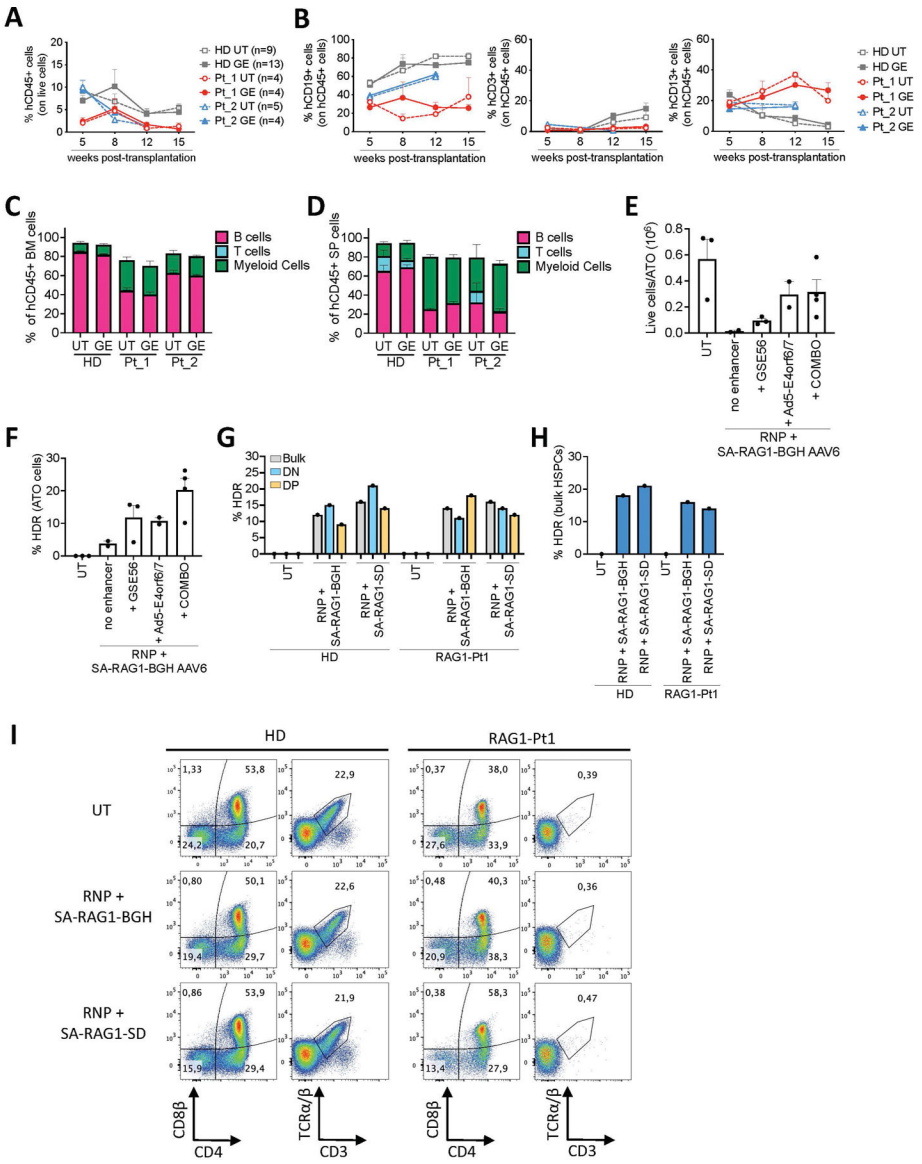

Figure 3. Suboptimal correction efficiency of intronic gene editing strategy in HD and RAG1-patient HSPCs

A. Kinetics of human CD45$^+$ engraftment in peripheral blood of NSG mice transplanted with HD and RAG1-patient mPB-HSPCs unedited (UT) or edited (GE) by g9/Cas9 RNP and SA-co.hRAG1-BGHpA AAV6 donor in presence of GSE56. **B.** Kinetics of human B cell (hCD19$^+$), T cell (hCD3$^+$) and Myeloid cell (hCD13$^+$) reconstitution in peripheral blood shown as proportion of total human CD45$^+$ cells. **C and D.** Immune cell composition in BM (**C**) and spleen (**D**) of NSG mice transplanted with unedited or edited HD and RAG1-patient mPB-HSPCs; sample size is shown in the legend of panel A. **E.** Number of live cells harvested 4 weeks after ATOs seeding with HD mPB-HSPCs edited by g9/Cas9 RNP and SA-co.hRAG1-BGHpA AAV6 donor in presence of different HDR-enhancers. **F.** Percentage of HDR-edited alleles measured in ATO-derived cells 4 weeks after ATOs seeding with mPB HD-HSPCs. **G-H.** Percentage of HDR-edited alleles measured in ATO-cells (6 weeks after ATOs seeding (**G**)) or in mPB-HSPCs (4 days after GE, **H**) derived from HD and

patients with RAG1 deficiency and edited by g9/Cas9 RNP and SA-co.hRAG1-BGHpA or SA-co.hRAG1-SD AAV6 donor in presence of GSE56 and Ad5-E4orf6/7. **I.** Representative plots of T-cell differentiation in ATOs (gated on live $CD45^{+}CD56^{-}$ cells) 6 weeks after the seeding with HD and RAG1-patients mPB-HSPCs untreated or edited by g9 and SA-co.hRAG1-BGHpA or SA-co.hRAG1-SD AAV6 donor in presence of GSE56 and Ad5-E4orf6/7.

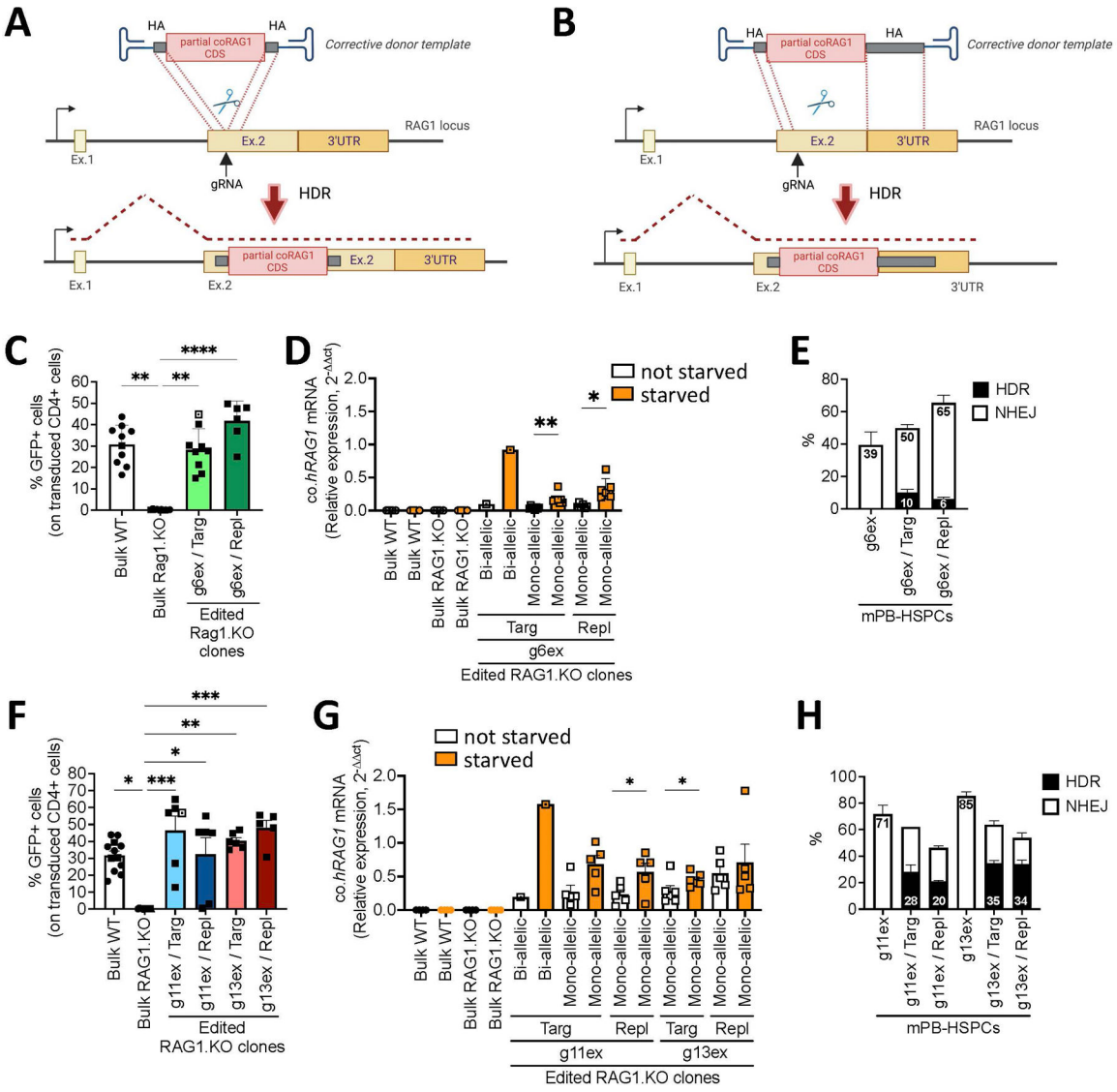

Figure 4. Functional correction of *hRAG1* expression and function mediated by exonic gene editing strategies

A and B. Schematic representation of the targeting (A) and replacement (B) gene editing strategies targeting *hRAG1* exon 2. Panels were created using www.BioRender.com. **C.** Graph shows proportion of GFP^+ cells measured 7 days after serum starvation by flow cytometry as surrogate of RAG1 recombination activity in unedited bulk NALM6-WT (Bulk WT), unedited bulk NALM6-RAG1.KO (Bulk RAG1.KO) cells and in NALM6-RAG1.KO clones edited by g6ex/Cas9 RNP and targeting (Targ) or replacement AAV6 donor (Repl). Square with dot is for bi-allelic clone; full-colored square symbols indicate samples assayed in parallel. One-way ANOVA, Kruskal-Wallis test was used to assess statistically significant differences. **D.** Expression of co.hRAG1 assessed before and 4 days after starvation in edited NALM6-RAG1.KO clones in parallel to unedited WT and NALM6-RAG1.KO controls. Wilcoxon matched-pair test was used to assess statistically significant differences. **E.** Editing efficiency in terms of percentage of NHEJ- and HDR- edited alleles was evaluated in HD mPB-HSPCs edited by g6ex/Cas9 RNP alone or transduced with targeting (Targ)

or replacement (Repl) corrective AAV6 donors. Mean values are shown into the columns (n of independent HDs = 3,4,4). **F.** Functional correction of RAG1 recombinase activity in NALM6-RAG1.KO clones edited by g11ex/Cas9 RNP and g13ex/Cas9 RNP with targeting or replacement AAV6 donors measured by GFP^+ cells 7 days after starvation induced by CDK4/6i. Square with dot is for bi-allelic clone; full-colored square symbols indicate samples assayed in parallel. One-way ANOVA, Kruskal-Wallis test was used to assess statistically significant differences. **G.** Expression of co.hRAG1 CDS assessed before and 4 days after starvation in edited NALM6-RAG1.KO clones. **H.** Editing efficiency in terms of percentage of NHEJ- and HDR- edited alleles evaluated in HD mPB-HSPCs edited by g11ex/Cas9 RNP or g13ex/Cas9 RNP alone or transduced with targeting (Targ) or replacement (Repl) corrective AAV6 donors. Mean values are shown into the columns (n of independent HDs: g11ex n=4, g11ex/Targ n=2, g11ex/Repl n=2, g13ex n=5, g13ex/Targ n=3, g13ex/Repl 3). *P* values are showed as: *≤0.05; **≤0.01; ***≤0.001; ****≤0.0001.

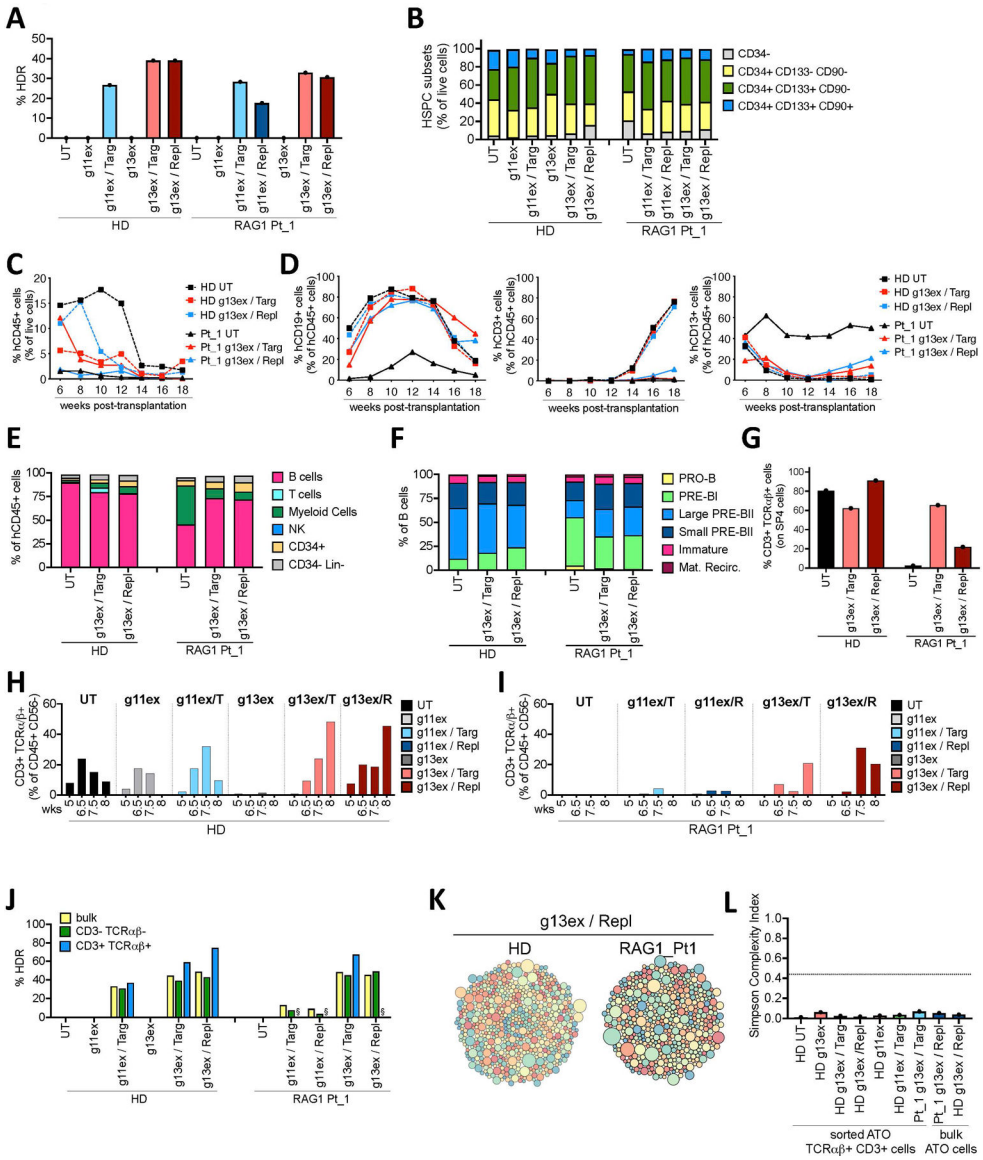

Figure 5. Functional rescue of hRAG1 defects by exonic gene editing of RAG1-patient HSPCs

A. Percentage of HDR-edited alleles measured by ddPCR 4 days after editing in HD and RAG1-patient mPB-HSPCs edited by g11ex/Cas9 or g13ex/Cas9 RNP and targeting (Targ) or replacement (Repl) AAV6 donor in the presence of editing enhancers (GSE56 and Ad5-E4orf6/7). **B.** Composition of unedited and edited HD and patient-derived HSPCs evaluated by flow cytometry 4 days after editing. **C.** Kinetics of human $CD45^+$ engraftment in peripheral blood of NSG mice transplanted with HD and RAG1-patient (Pt_1) mPB-HSPCs unedited (UT) or edited by g13ex/Cas9 RNP and targeting (Targ) or replacement (Repl) AAV6 donor in presence of editing enhancers. **D.** Kinetics of human B cell ($hCD19^+$), T cell ($hCD3^+$) and myeloid cell ($hCD13^+$) reconstitution in peripheral blood shown as proportion of total human $CD45^+$ cells. **E.** Hematopoietic cell composition in BM of transplanted NSG mice. **F**. Differentiation stages of B-cell lymphopoiesis in BM of transplanted NSG mice was evaluated by flow cytometry according to the following immunophenotype: Pro-B,

$CD34^{+}CD19^{-}CD22^{+}$; Pre-BI, $CD34^{+}CD19^{+}$; large Pre-BII, $CD34^{-}CD19^{+}CD10^{+}CD20^{-}$; small Pre-BII, $CD34^{-}CD19^{+}CD10^{+}CD20^{int}$; immature, $CD34^{-}CD19^{+}CD10^{+}CD20^{+}$; mature circulant, $CD34^{-}CD19^{+}CD10^{-}CD20^{+}$. **G.** Proportion of live $CD3^{+}TCR\alpha/\beta^{+}$ cells gated on single positive $CD4^{+}$ cells (SP4) was measured by flow cytometry in thymocytes isolated from transplanted NSG mice. **H and I.** Proportion of differentiated live $CD3^{+}TCR\alpha/\beta^{+}$ T cells was measured at indicated weeks (wks) in ATOs seeded with HD (**H**) and RAG1-patient (RAG1 Pt_1, **I**) mPB-HSPCs edited with g11ex or g13ex and targeting (/T) or replacement (/R) AAV6 donors in presence of editing enhancers. **J.** Percentage of HDR-edited alleles in sorted T-cell subsets harvested from ATOs 6 weeks after seeding. Analysis was not done in samples indicated by § asterisk because of few cell numbers. **K.** Packcircle plots displaying abundance of TCRB rearrangements in bulk cells harvested 7.5 weeks after ATO seeding with HD and RAG1-patient mPB-HSPCs edited by g13ex/Cas9 RNP and Replacement (Repl) AAV6 donor. **L.** Simpson complexity index measuring the sample clonality (ranging from 0 for a properly diverse population, to 1 for a monoclonal population) in $CD3^{+}TCR\alpha/\beta^{+}$ cells sorted 6.5 weeks upon ATO-seeding or in bulk ATO cells 7.5 weeks upon ATO-seeding.

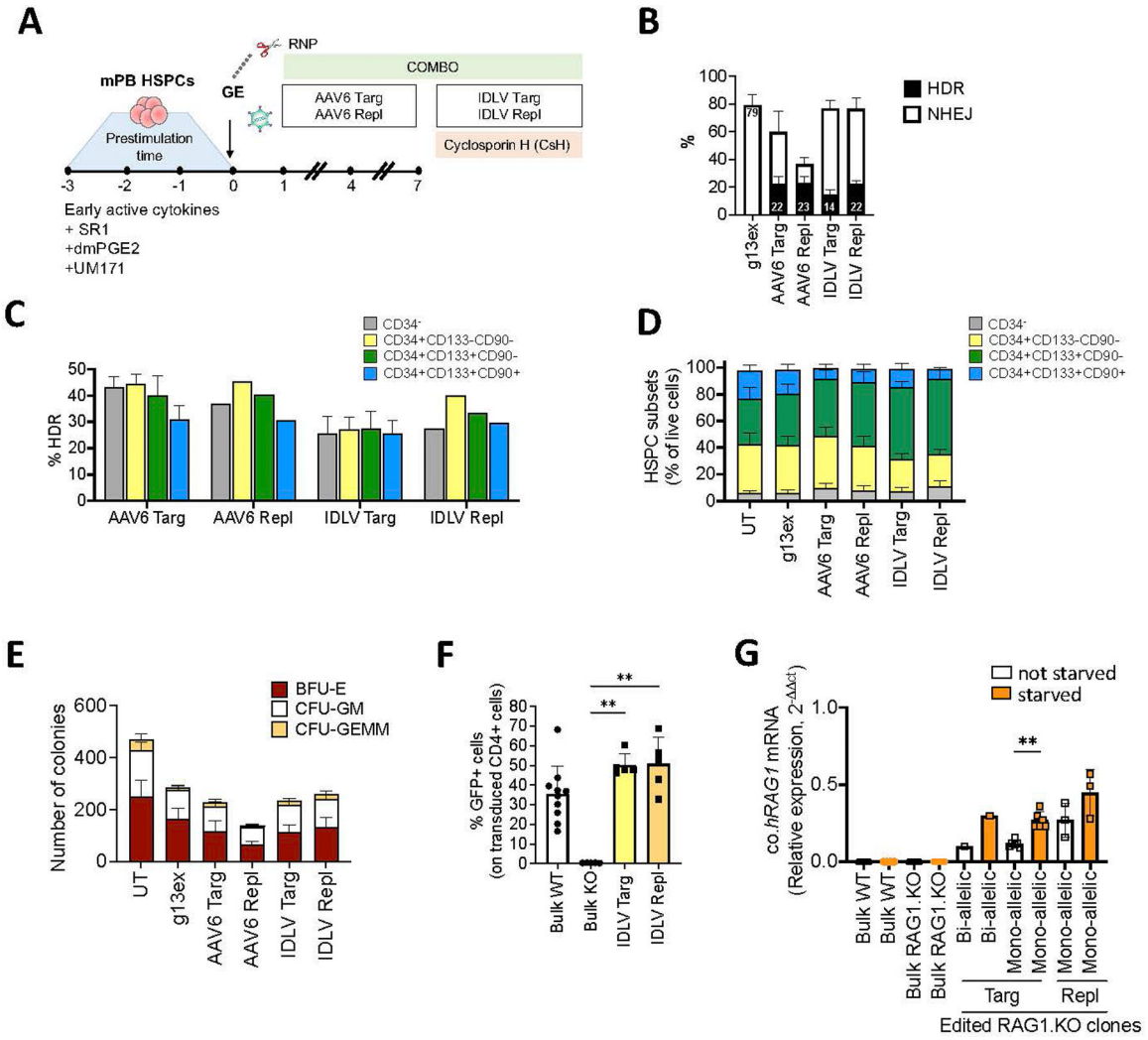

Figure 6. Comparison of AAV6 and IDLV as delivery platforms for RAG1 GE in HSPCs

A. Schematic representation of AAV6 and IDLV deliveries for the GE strategies targeting the hRAG1 exon 2. **B.** Editing efficiency in terms of percentage of NHEJ- and HDR- edited alleles evaluated in HD mPB-HSPCs edited by g13ex/Cas9 RNP alone or transduced with AAV6 and IDLV targeting (Targ) or replacement (Repl) corrective donors evaluated 4 days after editing. Mean values are shown into the columns (n. of independent HDs: g13ex n6, AAV6 Targ n=6, AAV6 Repl n=4, IDLV Targ n=6, IDLV Repl n=4). **C.** Percentage of HDR-edited alleles measured in sorted HSPC subsets, from the most committed ($CD34^-$) to the most primitive subpopulation ($CD34^+CD133^+CD90^+$). Mean values are shown into the columns (n of independent HDs: AAV6 Targ,n=3, AAV6 Repl n=1, IDLV Targ n=3, IDLV Repl n=1). **D.** Composition of unedited and edited HD HSPCs evaluated by flow cytometry 4 days after editing (n. of independent HDs: UT n=3, g13ex n=4, AAV6 Targ n=4, AAV6 Repl n=3, IDLV Targ n=4, IDLV Repl n=2. **E.** Number of colonies belonging to erythroid burst forming units (BFU-E), granulocyte-macrophage colony forming units (CFU-GM), and granulocyte, erythroid, macrophage, megakaryocyte units (CFU-GEMM). Mean values are shown into the columns (n. of independent HDs: UT n=4, g13ex n=4,

AAV6 Targ n=4, AAV6 Repl n=4, IDLV Targ n=4, IDLV Repl n=3. **F.** Graph shows proportion of GFP^+ cells measured 7 days after serum starvation by flow cytometry as surrogate of RAG1 recombination activity in unedited bulk NALM6-WT (Bulk WT), unedited bulk NALM6-RAG1.KO (Bulk RAG1.KO) cells and in NALM6-RAG1.KO clones edited by g13ex/Cas9 RNP and targeting (Targ) or replacement IDLV donor (Repl). One-way ANOVA, Kruskal-Wallis test was used to assess statistically significant differences. **G.** Expression of co.hRAG1 assessed before and 4 days after starvation in edited NALM6-RAG1.KO clones in parallel to unedited WT and NALM6-RAG1.KO controls. Wilcoxon matched-pair test was used to assess statistically significant differences. *P* values are showed as: *≤0.05; **≤0.01; ***≤0.001; ****≤0.0001.